ISMIP6-based Antarctic Projections to 2100: simulations with the BISICLES ice sheet model

James F. O'Neill[1], Tamsin L. Edwards[2], Daniel F. Martin[3], Courtney Shafer[4], Stephen L. Cornford[5], Hélène L. Seroussi[6], Sophie Nowicki[4], Mira Adhikari[2], and Lauren J. Gregoire[7]

[1]Centre for Geography and Environmental Sciences, University of Exeter, Penryn Campus, Cornwall, UK.
[2]Department of Geography, King's College London, London, UK.
[3]Computational Research Division, Lawrence Berkeley National Laboratory, Berkeley, CA, USA.
[4]Department of Geology, University at Buffalo, Buffalo, NY, USA.
[5]Centre for Polar Observation and Modelling, University of Bristol, Bristol, UK.
[6]Thayer School of Engineering, Dartmouth College, Hanover, NH, USA.
[7]School of Earth and Environment, University of Leeds, Leeds, UK

Correspondence: James O'Neill (j.oneill2@exeter.ac.uk)

Abstract. The contribution of the Antarctic ice sheet is one of the most uncertain components of sea level rise to 2100. Ice sheet models are the primary tool for projecting future sea level contribution from continental ice sheets. The Ice Sheet Model Intercomparison for the Coupled Model Intercomparison Phase 6 (ISMIP6) provided projections of the ice sheet contribution to sea level over the 21st century, quantifying uncertainty due to ice sheet model, climate model, emission scenario, and uncertain parameters. We present simulations following the ISMIP6 framework with the BISICLES ice sheet model, alongside new experiments extending the ISMIP6 protocol to more comprehensively sample uncertainties in future climate, ice shelf sensitivity to ocean melting, and their interactions. These results contributed to the land ice projections of Edwards et al. (2021), which formed the basis of sea level projections for the Sixth Assessment Report of the Intergovernmental Panel on Climate Change (AR6). We present BISICLES experiments showing the important interplay between surface mass balance processes and ocean driven melt in determining Antarctic sea level contribution. Under higher warming scenarios, high accumulation offsets more ocean driven mass loss, when sensitivity to ocean driven melt is low. Conversely, we show that when sensitivity to ocean warming is high, ocean melting drives increased mass loss despite high accumulation. Overall, we simulate a sea level contribution range across our experiments from 2 mm to 178 mm. Finally, we show that collapse of ice shelves due to surface warming increases sea level contribution by 25 mm, relative to the no collapse experiments, for both moderate and high sensitivity of ice shelf melting to ocean forcing.

1 Introduction

The Antarctic and Greenland ice sheets were the third largest contributor to global mean sea level (GMSL) change from 1901 to 2018, behind thermosteric changes and mountain glaciers (Palerme et al., 2017; Horwath et al., 2022; Fox-Kemper et al., 2021) – which together accounted for 79% of the 20 cm of sea level rise (Fox-Kemper et al., 2021). In recent decades, ice sheet mass loss has contributed a growing proportion of sea level rise, which averaged 3.64 ± 0.26 mm yr^{-1} between 2003 and 2016

(Horwath et al., 2022). From 1992 to 2020, the Antarctic ice sheet (AIS) contributed 7.4 ±1.5 mm to global mean sea level rise (Otosaka et al., 2023). Although Antarctica was a smaller source of GMSL between 1993 and 2016 than other land ice sources and land water storage (Horwath et al., 2022), evidence of past volume and dynamics suggest that the ice sheet could become a significant source of GMSL in a warming climate (DeConto et al., 2021; Lowry et al., 2021; Edwards et al., 2019). To date, mass loss in Antarctica has been dominated by the dynamic glacier response to warm ocean currents eroding ice shelves in the Amundsen Sea sector (Shepherd et al., 2018; Rignot et al., 2019), with changes in ocean currents linked to anthropogenic warming-driven changes to wind regimes (Holland et al., 2019). Along with some East Antarctic basins, the West Antarctic ice sheet may be vulnerable to ocean driven instabilities as grounding lines retreat into over-deepened subglacial basins (Schoof, 2012; Weertman, 1974; Thomas, 1979). Around 23 m of sea level equivalent Antarctic ice rests on bedrock below sea level (Morlighem et al., 2020).

Under anthropogenic warming, ice loss from marine basins could drive accelerating Antarctic GMSL contribution to 2100 and beyond (Schlegel et al., 2018; Bulthuis et al., 2019; Lowry et al., 2021; Edwards et al., 2019; DeConto and Pollard, 2016; Golledge et al., 2015; Ritz et al., 2015; Seroussi et al., 2024), amplifying uncertainty in future sea level projections (Robel et al., 2019). Alongside this ocean-driven retreat under anthropogenic warming, increased Antarctic snowfall accumulation, particularly over East Antarctica, has the potential to mitigate the ice sheet's sea level contribution. Warmer air temperatures over Antarctica can increase precipitation, driving increased surface mass balance under the cold, low melt conditions of the ice sheet (Frieler et al., 2015; Palerme et al., 2017). Over the course of the 20th century, increased precipitation offset ~10 mm of AIS-sourced GMSL (Medley and Thomas, 2019).

Ice sheet models are the primary tool for projecting future Antarctic sea level contribution. Over the past few decades, models have developed to represent a greater range of ice sheet processes and climate-ice sheet interactions, at higher resolution than ever before (Pattyn et al., 2017). However, differences in process representation, model physics, spatial discretisation and initialisation (Seroussi et al., 2019) mean that different ice sheet models project different AIS responses to the same climate boundary conditions (Edwards et al., 2014; Bindschadler et al., 2013). The Ice Sheet Model Intercomparison Project for the Coupled Modeled Intercomparison Projects Phase 6 (CMIP6), ISMIP6 (Nowicki et al., 2016), builds on previous multi-model ensemble efforts (e.g. Edwards et al. 2014; Bindschadler et al. 2013) to better characterise uncertainty in projected future GMSL from the Greenland and Antarctic ice sheets (Nowicki et al., 2016). With a common set of experiments run by different modelling groups, it allows for improved quantification of uncertainty in sea level projections due to choice of ice sheet model.

Results of ISMIP6 Antarctic ice sheet experiments forced with Coupled Model Intercomparison Project Phase 5 (CMIP5) climate models are described by Seroussi et al. (2020), who find a range of -7.8 cm to 30.0 cm sea level equivalent (SLE) contribution from Antarctica between 2015 and 2100 under a very high emissions scenario (RCP8.5) compared with experiments under constant climate conditions. Under a low emissions scenario (RCP2.6), an average additional mass loss of 0.0 to 3.0 cm is found based on two CMIP5 models compared with simulations under modern climate (Seroussi et al., 2020). Comparing these results with a further ensemble of simulations using next generation CMIP6 climate model forcings, Payne et al. (2021) find a limited difference between projections grouped by generation of CMIP climate model. This is attributed to the complexity of interactions between the AIS and the climate system, with warming-linked surface mass balance increases offsetting

ocean melt driven mass loss in some cases (Payne et al., 2021). Whilst CMIP6 models generally simulate more warming than CMIP5 models, both ocean melting and surface mass balance are enhanced in CMIP6, so that sea level contribution does not differ significantly by CMIP generation (Payne et al., 2021).

BISICLES ISMIP6 Antarctic experiments were used in the ISMIP6 synthesis and sensitivity tests of Edwards et al. (2021). However, with the exception of experiments for the model initialisation intercomparison exercise (InitMIP) (Seroussi et al., 2019), ISMIP6 BISICLES simulations have not yet been presented in detail (Edwards et al., 2021). We chose BISICLES to complement the original ISMIP6 ensemble experiments because of its use of adaptive mesh refinement and the L1L2 flow approximation (Cornford et al., 2013), making it well suited to simulating marine ice sheets (Cornford et al., 2015, 2016, 2020). This allows BISICLES to capture grounding line dynamics at high resolution, whilst maintaining computational efficiency.

We present here a set of 19 simulations (18 projections and a control) from the BISICLES ice sheet model following the ISMIP6 design for future projections of the Antarctic ice sheet. Our simulations follow the design for Tier 1, 2 and 3 experiments (Nowicki et al., 2016). Tier 1 are core ISMIP6 experiments, using climate forcing derived from the highest skill models identified in Barthel et al. (2020), exploring scenario dependence and sensitivity to shelf collapse and ice shelf basal melt sensitivity (Nowicki et al., 2016). Tier 2 experiments explore a wider range of models assessed in Barthel et al. (2020) from the CMIP5 ensemble, as well as CMIP6 models based on availability. Tier 3 experiments provide a more in-depth exploration of the role of ocean sensitivity in modelled AIS evolution to complement Tier 1 (Nowicki et al., 2016).

We also explore the relationship between ocean melt and ice shelf collapse through additional sensitivity experiments. The Tier 1-3 experiments contribute to the ISMIP6 effort by adding another Antarctic ice sheet model to the ensemble, while the additional sensitivity experiments target uncertainties in the synthesis by Edwards et al. (2021): by testing for interactions between uncertain parameters.

Here we present the BISICLES model set-up and experimental design (Section 2) and results of the 19 ice sheet model experiments (Section 3). We then discuss the role of different modelling choices on Antarctic contribution to sea level, compare BISICLES to other ISMIP6 ice sheet models, and finally discuss limitations of our approach (Section 4).

2 Methods

2.1 BISICLES

BISICLES is a block-structured, finite volume, ice sheet model solving the L1L2 flow approximation with adaptive mesh refinement (Cornford et al., 2013, 2015, 2016) (supplementary Section 1.1). For these simulations, we use the BISICLES_B model set up as in Seroussi et al. (2019) and the same initial state. All simulations are run with a base resolution of 8 km, with 3 levels of refinement to reach a finest mesh resolution of 1 km (supplementary Figure 1). The model domain at the coarsest level covers a grid of 768 x 768 cells. We use the subgrid friction interpolation scheme described in Cornford et al. (2016). This allows for finest resolution of 1 km at the grounding line and in regions of fast flowing ice, adequately capturing grounding line dynamics compared with higher resolution simulations where the subgrid friction scheme is not used (Cornford et al., 2016).

Basal sliding is calculated using a pressure-limited Weertman-Coulomb type law (Tsai et al., 2015) with m=1/3 and a Coulomb friction coefficient of 0.5. This sliding law accommodates regions of hard beds and slow flow through the Weertman law, and regions of faster flow on deformable beds through the Coulomb law, as well as a smooth transition between the two (supplementary Section 1.1, equation 6). Basal traction coefficients and the effective viscosity coefficient (ϕ) are estimated using an inversion approach to minimise the mismatch between modelled ice velocity and observations collected between 2007 and 2010 (Cornford et al., 2015), and are held constant throughout the simulations. Ice temperature is from Pattyn et al. (2010), who simulated ice sheet temperature with a 3D thermo-mechanical ice sheet model, and is fixed throughout the simulations. Whilst BISICLES uses a depth integrated momentum balance equation, the rate factor A(T) in effective viscosity is based on 3D ice temperature (supplementary Section 1.1, equation 5). The inverted parameter ϕ corrects the vertically integrated effective viscosity in essentially the same way as a damage parameter D (phi = 1 – D) (supplementary Section 1.1, equation 3), but will conflate the influence of errors in the ice temperature and thickness, as well as the form of the rate factor. In the experiments presented here, the calving front is fixed with the exception of collapse on experiments, where ice shelf is removed based on collapse masks (see next section). However, ice thinner than 1 m is automatically calved. All simulations are initialised from a nine year relaxation run, as in previous BISICLES studies (Cornford et al., 2016) (supplementary Section 1.3). Whilst the ISMIP6 analysis period is from 2015 to 2100, our simulations start in 2010 and use the ISMIP6 forcing anomalies provided, which cover the period 1995-2100.

Ice sheet contribution to sea level is caculated from the change in ice volume above floatation (VAF) in the absence of bedrock deformation - a process we do not include. Volume above floatation is the volume of ice sheet that is not below sea level or hydrostatic equilibrium, and is therefore not already displacing ocean water. To calculate sea level contribution, i.e. change in VAF in metres sea level equivalent (m SLE) for the modern ocean, we distribute sea level equivalent change in VAF over an ocean area of 3.625×10^{14} m^2 (Gregory et al., 2019), with ocean density 1028 kg m^{-3} and ice density 918 kg m^{-3} (Goelzer et al., 2020). As we use an inversion approach, some retreat in our model is due to dynamic retreat not driven by climate, which is none-the-less an important component of the ice sheets future sea level contribution. We therefore present our results without subtracting the control sea level contribution.

2.2 Ocean and atmosphere forcing

We use the three models identified in Barthel et al. (2020) as having the highest skill in simulating climate variables, whilst sampling a diverse subset of CMIP5 climate models. These are NorESM1-M, CCSM4 and MIROC-ESM. Additionally, we use one CMIP6 model in our simulations - CNRM-CM6-1, as forcing data were available to us for both low (SSP1.26) and high (SSP5.85) emissions scenarios, which was not the case for other CMIP6 models. We can therefore explore scenario dependence across a wider range of GCMs, and across CMIP generations.

To promote a consistent approach to basal melt forcing across ice sheet models, most participating groups used a prescribed basal melt parameterisation (Jourdain et al., 2020; Nowicki et al., 2020). This parameterisation describes the relationship between basal melting, m, and ocean thermal forcing, TF. BISICLES implements the "non-local" basal melt rate parameterisation. Basal melt anomalies, relative to the initial melt forcing, are applied for each simulation year. The non-local basal melt

parameterisation captures the melt-induced cavity scale circulation changes that drive shelf melt (Jourdain et al., 2017), as well as the local influence of stratification, and compares favourably to coupled ice sheet ocean models in idealised experiments (Favier et al., 2019). A more comprehensive description can be found in Jourdain et al. (2020). It is restated here:

$$\begin{aligned} m(x,y) =& \gamma_0 \times \left(\frac{\rho_{sw} C_{pw}}{\rho_i L_f}\right)^2 \\ & \times (TF(x,y,z_{draft}) + \delta T_{sector}) \\ & \times |\langle TF \rangle_{draft \in sector} + \delta T_{sector}|, \end{aligned} \tag{1}$$

where ρ_i and ρ_{sw} are the densities of ice (918 kg m^{-3}) and sea water (1028 kg m^{-3}) respectively; L_f is the fusion latent heat of ice (3.3 $\times$ 10^5 J kg^{-1}); and C_{pw} is the specific heat of sea water (3974 J kg^{-1} K^{-1}). The thermal forcing, TF, is calculated at the ice-ocean interface, while $\langle TF \rangle$ is averaged over each of the 16 Antarctic sectors. Figure 1 shows thermal forcing averaged over the surface ocean (0 - 500 m) from 2015 to 2100 for the GCMs used here.

The basal melt parameter, γ_0, is calibrated using two sets of melt estimates to span a wide range of possible sensitivities of the ice shelves to basal melt as outlined in Jourdain et al. (2020). The two sets of melt estimates are based on total Antarctic basal melt (Depoorter et al., 2013; Rignot et al., 2013) (*MeanAnt*) and melting at the grounding line of Pine Island Glacier (*PIGL*), respectively (Jourdain et al., 2020). In all, six values of γ_0 are provided (Table 1), corresponding to the 5^{th}, 50^{th} and 95^{th} percentiles of the distribution for the low (*MeanAnt*) and high (*PIGL*) melt tuning. Five γ_0 values are sampled in the simulations presented here (Table 2). With limited time and computational resources, we did not use $PIGL_{5th}$, prioritising instead higher γ_0 simulations to bound the ice sheet sensitivity to ice shelf basal melting. Basal melting is only applied to cells whose centre is at floatation.

Calibration	5^{th}	Median	95^{th}
$MeanAnt$	9,620	14,500	21,000
$PIGL$	88,000	159,000	471,000

Table 1. Calibrated values of basal melt parameter, γ_0, in m yr^{-1}

For the ice/ atmosphere interface, surface mass balance anomalies were provided directly from GCMs relative to a January 1995 to December 2014 reference period (Nowicki et al., 2016). The anomalies were added to a baseline surface mass balance from Arthern et al. (2006) following previous BISICLES studies (Cornford et al., 2016) and BISICLES initMIP experiments (Seroussi et al., 2019). This approach does not account for the evolving topography of Antarctica over the simulation period. Average surface mass balance anomalies for 2015 to 2100 are shown in Figure 2.

Surface melt water can enhance propagation of crevasses in ice shelves, driving weakening and eventual collapse (Scambos et al., 2009). However, inclusion of melt-driven hydrofracture, subsequent shelf collapse and unstable grounded ice retreat is a relatively recent innovation in ice sheet models (Pollard et al., 2015). Questions remain around collapse mechanisms and resulting rate of retreat (Crawford et al., 2021), as well as the importance of these mechanisms for past (Edwards et al.,

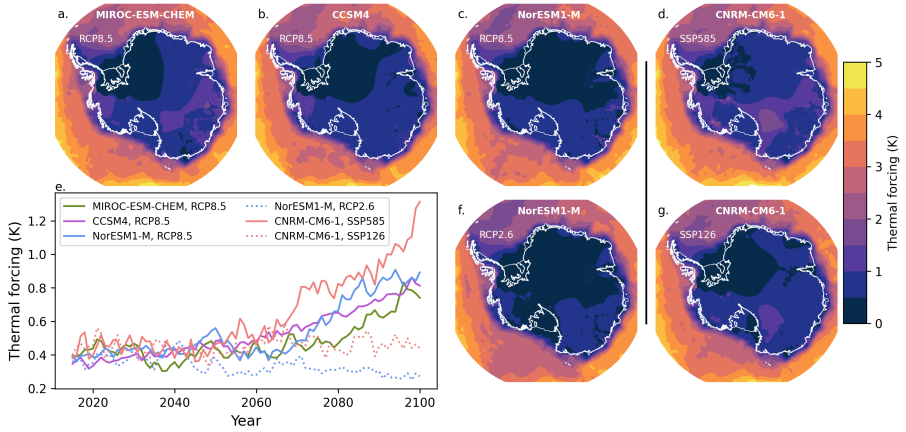

Figure 1. Thermal forcing averaged over the upper ocean (0 - 500 m) from 2015 to 2100 for MIROC-ESM under RCP8.5 (**a**), CCSM4 under RCP8.5 (**b**), NorESM1-M under RCP8.5 (**c**), NorESM1-M under RCP2.6 (**f**), CNRM-CM6-1 under SSP5.85 (**d**) and CNRM-CM6-1 under SSP1.26 (**g**). Subplot **e** shows Antarctic mean annual upper (0 - 500 m) ocean thermal forcing from 2015 to 2100. Black vertical line separates CMIP5 models (under RCP scenarios) from the CMIP6 model (SSP scenarios).

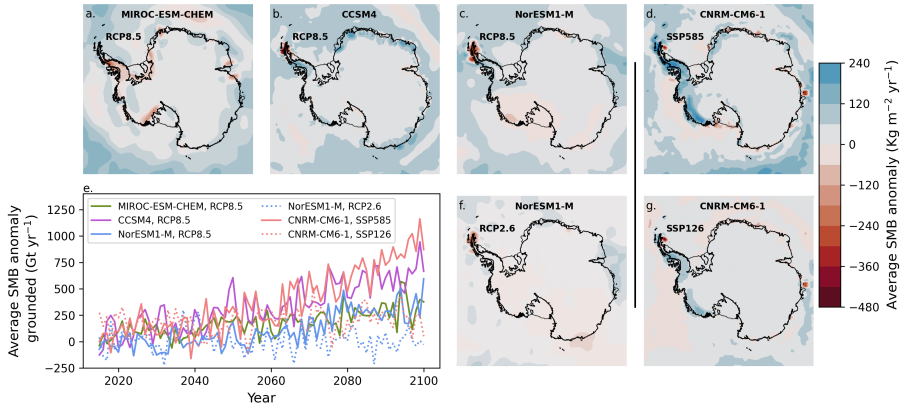

Figure 2. Surface mass balance anomaly (relative to 1995-2014) averaged from 2015 to 2100 for MIROC-ESM under RCP8.5 (**a**), CCSM4 under RCP8.5 (**b**), NorESM1-M under RCP8.5 (**c**), NorESM1-M under RCP2.6 (**f**), CNRM-CM6-1 under SSP5.85 (**d**) and CNRM-CM6-1 under SSP1.26 (**g**). Subplot **e** shows Antarctic mean annual surface mass balance anomaly from 2015 to 2100. Black vertical line separates CMIP5 models (under RCP scenarios) from the CMIP6 model (SSP scenarios).

2019) and future 21st century (Morlighem et al., 2024) Antarctic stability. Hydrofracture-driven shelf collapse is not directly implemented in those models participating in ISMIP6. ISMIP6 therefore provide time-dependent masks of ice shelf collapse to represent surface melt-enhanced ice shelf disintegration. The masks are derived from atmospheric forcing projections: if surface air temperature-driven melt of 725 mm a^{-1} water equivalent persists for 10 years, the ice shelf is removed (Trusel et al., 2015; Seroussi et al., 2020).

We explore the impact of shelf collapse with two pairs of experiments (Table 2). Both sets of 'collapse on' simulations use the same shelf collapse mask, i.e., derived from the same climate model projections (CCSM4). In these experiments, shelf collapse progresses southward during the experiment, from the Antarctic Peninsula towards the South pole. In these experiments, ~30% of the original Bedmap2 ice shelf area is removed by 2100.

2.3 Control simulation

The ISMIP6 protocol subtracts a control simulation from each projection simulation, to remove model drift (Nowicki et al., 2016) and more easily compare results from different ice flow models with varying drifts. Our control simulation uses the Arthern et al. (2006) surface mass balance forcing. Basal melting is applied such that localised thickening - as a result of ice advection or surface mass balance - is removed. Basal melt driven by ocean thermal forcing is not applied, and accumulation onto the lower surface is not permitted (see BISICLES_B in Seroussi et al. (2019)). Ice shelves can thin locally due to advection of ice out of grid cells. Treating the background melt field in this way maintains constant shelf thickness in most areas, but ensures that the large melt rates immediately downstream from the grounding line are maintained, should the grounding line advance or retreat. Control experiment boundary conditions are detailed further in supplementary Section 1.4.

3 Results

3.1 Control simulation results

From 2015 to 2100, the control simulation loses 19,220 Gt of mass above floatation, contributing 53 mm to sea level (Fig. 3c). The ice sheet area decreases by 6.9×10^3 km^2, while the floating area increases by 64.6×10^3 km^2.

Thinning occurs over large regions of the Amundsen Sea sector, with some grounding line retreat on Thwaites Glacier (Fig. 3a). Major ice shelves (Ross, Ronne-Filchner and Amery) also thin, along with their tributary ice streams. However, thinning of Lambert Glacier (Fig. 3b) is less pronounced than in some ice streams on the Siple coast or those feeding the Ronne-Filchner shelf, consistent with a limited response of this catchment to ice shelf thinning in previous studies e.g. Gong et al. (2014). In East Antarctica, ice streams at the margins around Totten and the Wilkes basin (Fig. 3c) all undergo thinning in the control experiment.

The most pronounced ice stream speed up in the control simulation occurs in the Thwaites glacier and its ice shelf (Fig. 3f), in response to grounding line retreat. By contrast, Pine Island glacier slows down between 2015 and 2100 in the control run (Fig. 3f). Along the Siple coast, Whillans ice stream (Ice Stream B) accelerates between 2015 and 2100, with grounding lines

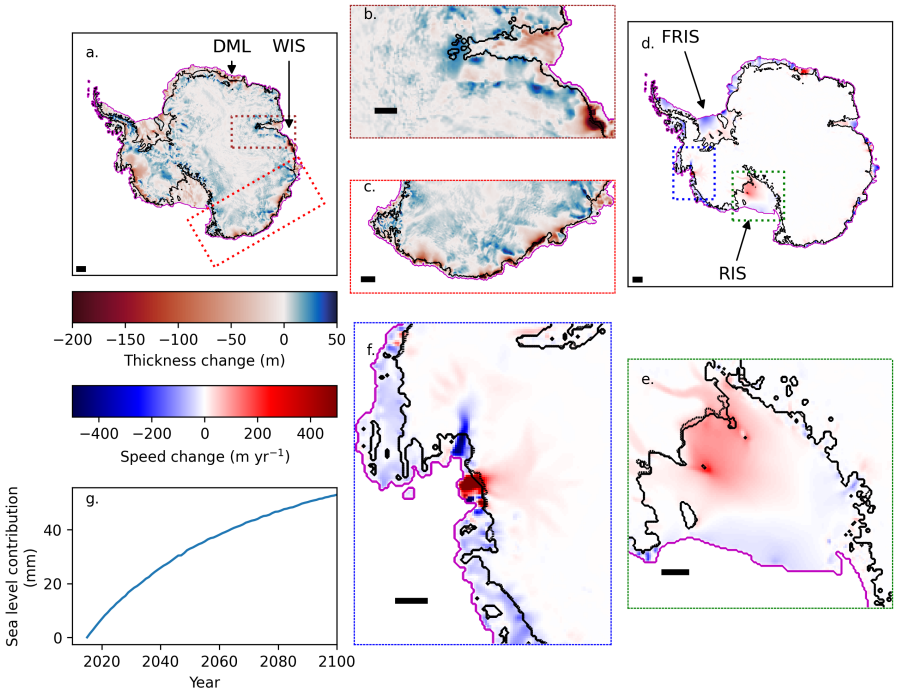

Figure 3. Control simulation (2015-2100). Subplot **a** shows thickness change between 2015 and 2100 in metres for the Antarctic ice sheet. Locations mentioned in the main text are indicated by arrows, Dronning Maud Land (DML) and the West Ice Shelf (WIS). Subplot **b** focuses in on thickness change in the Amery ice shelf and Lambert glacier, and corresponds to the brown dashed box in **a**. Subplot **c** shows thickness change for East Antarctica in the region of Totten glacier and the Wilkes basin, and corresponds to the red dashed box in **a**. Subplot **d** shows the change in ice speed between 2015 and 2100 in m yr^{-1}. The major ice shelves (Filchner-Ronne Ice Shelf: FRIS, Ross Ice Shelf: RIS) are indicated by arrows. Subplot **e** highlights speed change for the Ross ice shelf and Siple coast glaciers, and corresponds to the green dashed box in **d**. Subplot **f** highlights speed change for the Amundsen Sea Embayment glaciers, and corresponds to the blue dashed box in **d**. Subplot **g** shows the sea level contribution for the control simulation. Black scale bars in **a-f** correspond to 100 km. Black solid contour on **a-f** show 2015 grounding line position, black dotted contour shows 2100 grounding line position. Purple contour on subplots **a-f** shows 2015 shelf edge position.

Experiment	Scenario	GCM	γ_0 (m a^{-1})	γ_0 percentile	Collapse	SLC - control (mm)	SLC (mm)
control	-	-	-	-	OFF	-	53
exp05	RCP8.5	NorESM1-M	14,477	$MeanAnt_{50}$	OFF	31	84
exp06	RCP8.5	MIROC-ESM	14,477	$MeanAnt_{50}$	OFF	-2	51
exp07	RCP2.6	NorESM1-M	14,477	$MeanAnt_{50}$	OFF	38	91
exp08	RCP8.5	CCSM4	14,477	$MeanAnt_{50}$	OFF	-45	8
exp09	RCP8.5	NorESM1-M	21,005	$MeanAnt_{95}$	OFF	39	92
exp10	RCP8.5	NorESM1-M	9,619	$MeanAnt_{5}$	OFF	23	76
exp12	RCP8.5	CCSM4	14,477	$MeanAnt_{50}$	ON	-20	33
exp13	RCP8.5	NorESM1-M	159,188	$PIGL_{50}$	OFF	82	135
expD52	RCP8.5	NorESM1-M	471,264	$PIGL_{95}$	OFF	91	144
expD53	RCP8.5	MIROC-ESM	159,188	$PIGL_{50}$	OFF	71	124
expD55	RCP8.5	MIROC-ESM	471,264	$PIGL_{95}$	OFF	121	174
expD56	RCP8.5	CCSM4	159,188	$PIGL_{50}$	OFF	31	84
expD58	RCP8.5	CCSM4	471,264	$PIGL_{95}$	OFF	102	155
expT71†	RCP2.6	NorESM1-M	159,188	$PIGL_{50}$	OFF	62	115
expT73†	RCP2.6	NorESM1-M	471,264	$PIGL_{95}$	OFF	57	110
expTD58†	RCP8.5	CCSM4	471,264	$PIGL_{95}$	ON	125	178
expB6	SSP5-8.5	CNRM-CM6-1	14,477	$MeanAnt_{50}$	OFF	-53	2
expB7	SSP1-2.6	CNRM-CM6-1	14,477	$MeanAnt_{50}$	OFF	-17	53

Table 2. Experiment list with projected sea level contribution minus the control simulation from 2015 to 2100, and sea level contribution without the control subtracted - as quoted in the main text. The †symbol indicates new experiments that were not part of the ISMIP6 protocol.

in this sector undergoing modest retreat (Fig. 3e). Overall, outer edges of major ice shelves slow down over the simulation period, with the exception of some ice shelves on the Dronning Maud Land and the West Ice shelf (Fig. 3d). In these latter sectors, localised grounding line retreat is associated with speed up of ice across the grounding line and out to the shelf edge.

3.2 Projected sea level contribution

Projected sea level contribution from 2015-2100 varies between 2 mm and 178 mm across the 18 experiments (Table 2; Fig. 4). Five have a smaller sea level contribution than the control. All of these use the lower basal melt ($MeanAnt$) parameterisation, and are forced by two of the four GCMs (CCSM4 from CMIP5 and CNRM-CM6-1 from CMIP6), and four of the five are under very high emissions scenarios (RCP8.5 or SSP5-8.5).

3.3 Projected changes in ice area

Grounded ice sheet area changes are shown in Figure 5, grouped by GCM forcing. All simulations lose grounded area by 2100, with the exception of those forced by NorESM1-M under low emissions (RCP2.6) using the high basal melt parameterisation ($PIGL_{95}$), though under $PIGL_{50}$ and $PIGL_{95}$ the decrease is not monotonic. Perhaps counter-intuitively, initial grounded area increases with greater basal melt sensitivity to thermal forcing (i.e., higher values of γ_0: darker colours in Fig. 5). The

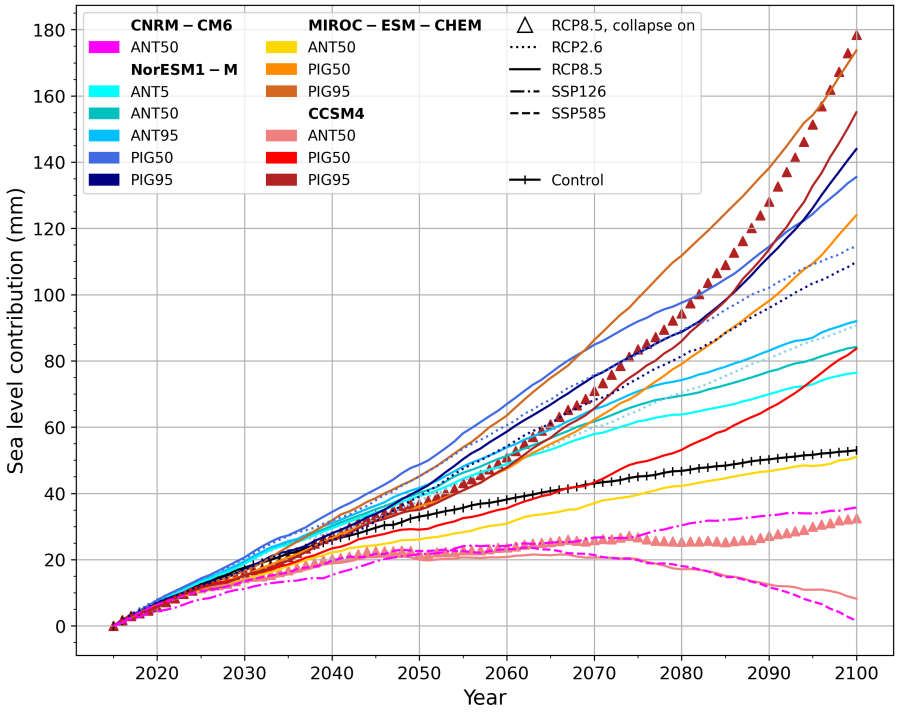

Figure 4. Sea level contribution (mm) for all experiments from 2015 to 2100.

differences in experiments between $MeanAnt$ percentiles are small because the γ_0 values are relatively similar (Table 1). However, high basal melt sensitivity ($PIGL$) experiments decrease in grounded area much more quickly, generally to smaller final values than the $MeanAnt$ experiments despite their larger areas in 2015.

In contrast, floating ice area is larger at 2100 compared with 2015 for all experiments, with the exception of those with ice shelf collapse (CCSM4: triangles in Fig. 6) and the experiment forced with NorESM1-M under RCP2.6 using the high basal melt parameterisation ($PIGL_{95}$). This response - i.e. reduced grounded ice sheet area and increased floating area - is consistent with grounding line retreat and loss of volume above floatation, with fixed front calving maintaining the shelf edge position so floating area increases as ice ungrounds. For collapse on experiments, loss of floating area from shelf collapse is partially offset by increases from grounding line retreat. Haseloff and Sergienko (2018) show that ice shelf buttressing can stabilise grounding lines, including on reverse sloping beds. Our fixed-front calving approach may therefore under-predict sea level contribution, particularly for buttressed ice streams such as Pine Island. Moreover, lack of calving may maintain buttressing, and could contribute to ice shelf slow-down in the control.

3.4 Regional sea level contributions

To explore the distinct responses of the West Antarctic ice sheet (WAIS), East Antarctic ice sheet (EAIS) and the Antarctic Peninsula (AP) to perturbed boundary conditions and basal melt sensitivity, we separate sea level equivalent mass change for

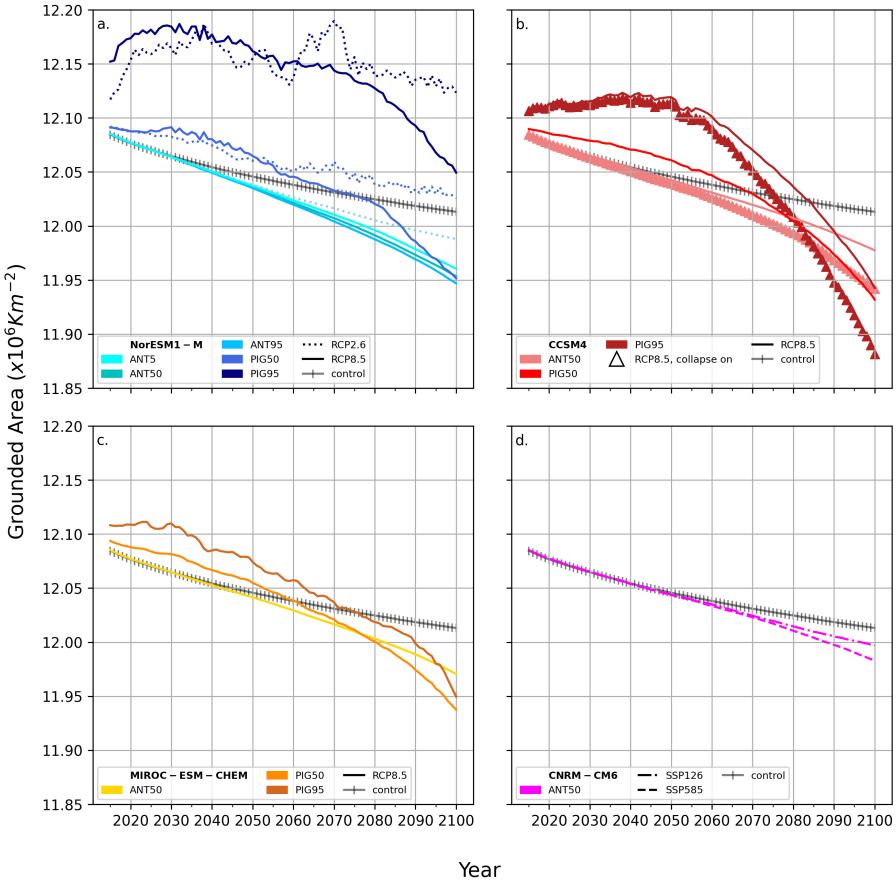

Figure 5. Grounded ice sheet area for all simulations from 2015 to 2100. Darker colours indicate higher γ_0 values. Subplots show the grounded area for NorESM1-M (**a**), CCSM4 (**b**), MIROC-ESM-CHEM (**c**) and CNRM-CM6 (**d**) experiments from 2015 to 2100.

these three regions (Fig. 7, supplementary Table 1). For WAIS, sea level contribution ranges from 15 mm to 139 mm (Fig. 7a). Two simulations have a smaller WAIS sea level contribution than the control. Projected sea level contribution for the EAIS ranges from 65 mm to -32 mm (Fig. 7b). Four simulations gain mass in the EAIS, and six have a smaller sea level contribution than the control. Projections of Antarctic Peninsula sea level contribution range from -3 mm to 13 mm (Fig. 7b), and ten experiments have a smaller sea level contribution than the control.

To further partition SLE ice sheet mass change, results are presented for the 16 drainage basins defined by Jourdain et al. 2020 (Fig. 8). The Amundsen Sea Embayment (ASE) sector (Fig. 8-10) has the largest sea level contribution of all 16 basins in 10 experiments, ranging from 21 mm to 62 mm (supplementary Table 1). This reflects patterns of thinning in the region across all experiments (supplementary Fig. 5). It exceeds the control sea level contribution in all but two experiments. With a sea level contribution of 26 mm, the ASE undergoes the largest mass loss in the control experiment. The Totten sector (Fig. 8-5) has the largest sea level contribution of any sector in 8 experiments, and sea level contribution ranges from 9 mm to 52

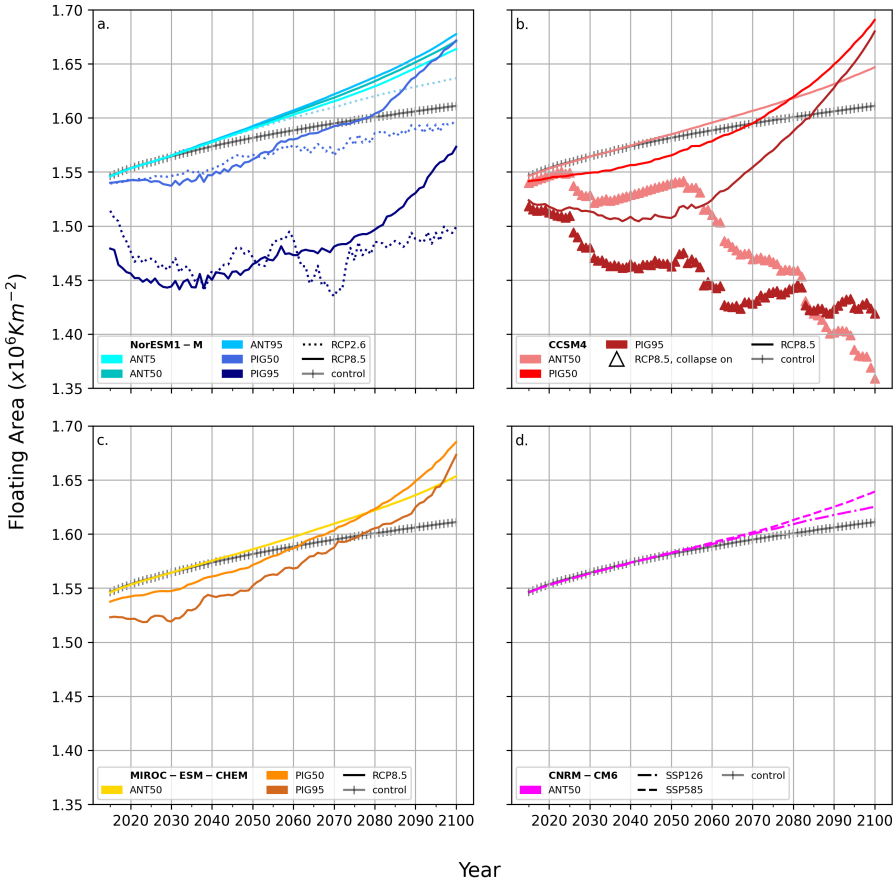

Figure 6. Floating ice sheet area for all simulations from 2015 to 2100. Darker colours indicate higher γ_0 values. Subplots show the grounded area for NorESM1-M (**a**), CCSM4 (**b**), MIROC-ESM-CHEM (**c**) and CNRM-CM6 (**d**) experiments from 2015 to 2100.

mm, with grounded ice thinning here in all experiments (supplementary Fig. 5). It exceeds the control sea level contribution in all but one experiments.

In the Filchner-Ronne sector (Fig. 8-15), fourteen simulations increase their VAF up to -21 mm sea level contribution. The Filchner-Ronne drainage basin has a large area over which to accumulate mass, which offsets mass loss due to ocean melting. However, the Filchner-Ronne sector loses mass equivalent to a 35 mm sea level contribution under high basal melt sensitivity and CCSM RCP8.5, giving it the largest projected range of any sector. The projected range in this sector illustrates the competing processes of increased accumulation under warming on the one hand (Payne et al., 2021) and increased mass loss due to basal melting on the other. When sensitivity to ocean melt is low, increased accumulation dominates ocean melt-driven mass loss. Conversely, under higher ocean melt sensitivity, ocean melt-driven mass loss counteracts the warming-driven negative surface mass balance (SMB) feedback. The importance of this compensation effect in determining the Filchner-Ronne sector sea level contribution has been demonstrated previously, for example in Cornford et al. (2015) and Wright et al. (2014).

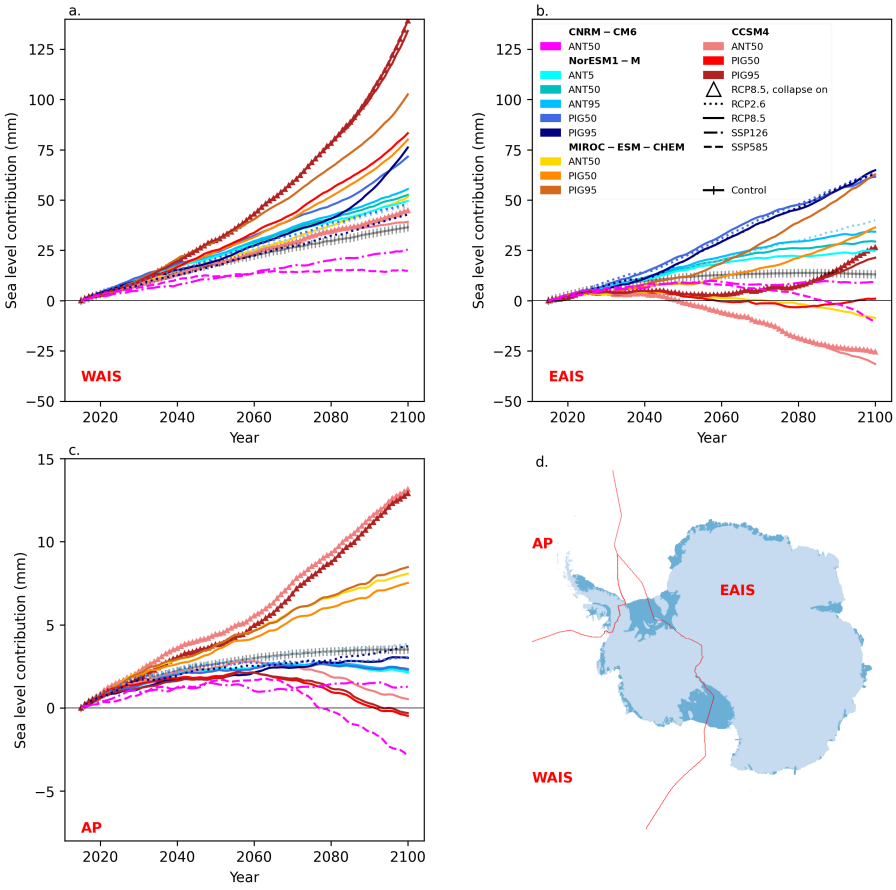

Figure 7. Sea level contribution (loss of volume above floatation) (mm) for the East Antarctic ice sheet (EAIS), West Antarctic ice sheet (WAIS) and Antarctic Peninsula (AP) from 2015 to 2100. Inset plot shows mask boundaries used to calculate regional change in volume above floatation. We note that the AP subplot has a truncated Y-axis compared with the WAIS and EAIS subplots to aid legibility.

Under the highest basal melt sensitivity, the loss of VAF in the Filchner-Ronne sector is 55 mm greater than under equivalent lower ocean sensitivity scenarios with the same forcing (supplementary Table 1).

The other sector with a major ice shelf, the Ross Sea sector (Fig. 8-8), gains mass in all but four experiments, with a sea level contribution range of -26 mm to 14 mm, with highest contribution under NorESM1-M RCP8.5 and the second highest basal melt sensitivity (supplementary Table 1). For the two highest sea level contribution experiments for the Filchner-Ronne sector (CCSM4, RCP8.5, highest basal melt sensitivities), the Ross sea sector contributes 9 mm to sea level. Mass gain for the major ice shelf sectors, despite ice shelf thinning and reduced buttressing (supplementary Fig. 5) in most experiments, reflects the large contribution to mass gain from accumulation over their grounded area.

For ISMIP6, participating models subtract the control simulation to account for model drift. However, the large sectoral contribution in our experiment suggests that this removes the sea level signal from the ASE's long timescale response to retreat

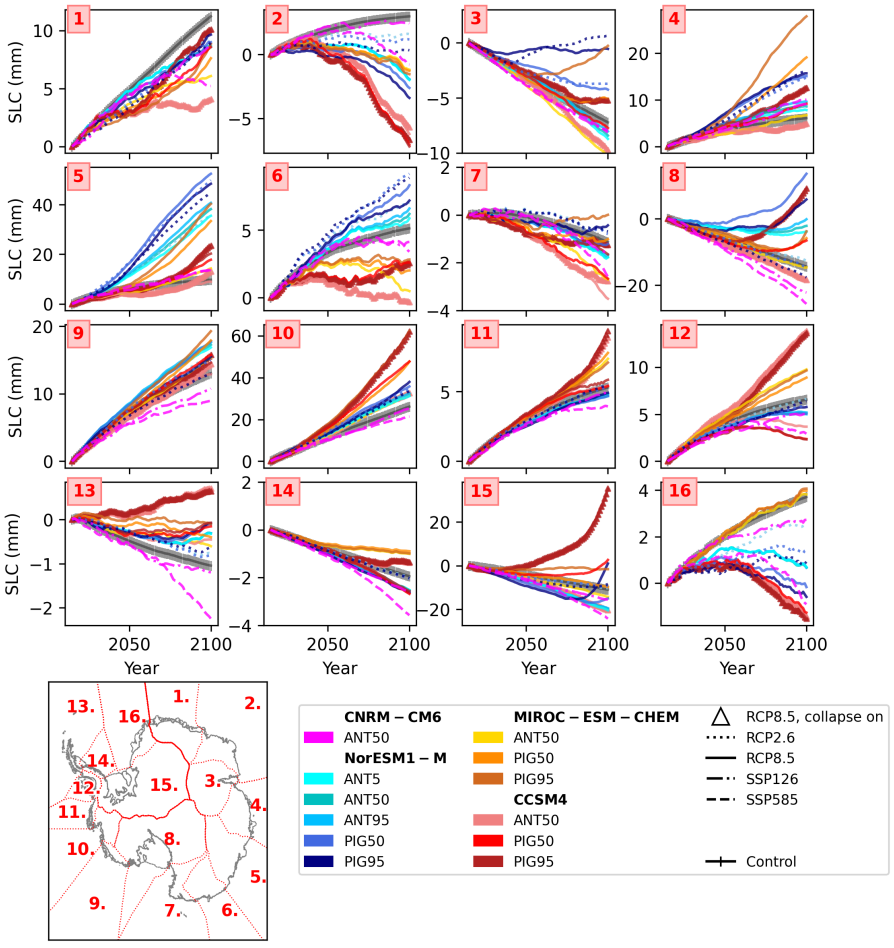

Figure 8. Sea level contribution by sector for all simulations. Basins are numbered are as follows: 1: Dronning Maud Land; 2: Enderby Land; 3: Lambert Glacier catchment; 4: Wilhelm II land; 5: Totten Sector; 6: George V Land; 7: Oates Land; 8: Ross Ice Shelf; 9: Getz ice shelf sector; 10: Amundsen Sea Embayment sector; 11: Abbott ice shelf sector; 12: George VI ice shelf sector; 13: Larsen sector; 14: Palmer Land; 15: Filchner-Ronne sector; 16: Brunt ice shelf sector. Note the different y-axis.

initiated before 2015. It is not clear that marine ice sheet instability has been initiated in the ASE, with the IPCC AR6 stating that observed flow regimes in the ASE are compatible with but not incontrovertible evidence of MISI (Fox-Kemper et al., 2021). In contrast, both the Ross Sea and Filchner-Ronne sectors steadily increase in VAF throughout the control simulation - broadly consistent with 1979- 2019 VAF trend in these regions (Rignot et al., 2019).

3.5 Dependence on GCM forcing

GCM-dependence is driven by patterns of surface mass balance over the ice sheet (Fig. 9c, d, f) and patterns of ocean forcing - the main driver of ice shelf thinning and increased grounding line flux (Fig. 9a, b, e).

To explore this, we compare simulations with the same ice shelf basal melt sensitivity under the same emissions scenario. Under the $MeanAnt_{50}$ tuning and RCP8.5, the NorESM1-M forced simulation contributes 84 mm to sea level, MIROC-ESM contributes 51 mm to sea level and CCSM4 has a sea level contribution of 8 mm. Of these three GCMs under RCP8.5, CCSM4 has highest SMB over WAIS and EAIS, followed by MIROC-ESM then NorESM1-M (Fig. 9c and d). Moreover, for MIROC-ESM and CCSM4, EAIS drives sea level fall, whilst the region loses mass under NorESM1-M (Fig. 7: pink (CCSM4), yellow (MIROC-ESM), turquoise (NorESM1-M) solid lines). This reflects the smaller response in the NorESM1-M atmosphere to RCP8.5 warming compared with other CMIP5 models (Barthel et al., 2020), which limits the extent to which warming-driven increases in surface mass balance compensate ocean-driven losses.

When higher basal melt sensitivity ($PIGL_{50}$) is used under the same emissions scenario, NorESM1-M again has the largest sea level contribution at 135 mm. The MIROC-ESM forced simulation contributes 124 mm to sea level, followed by CCSM4 with a sea level contribution of 84 mm. Under the highest basal melt sensitivity ($PIGL_{95}$), MIROC-ESM drives the largest sea level contribution at 174 mm, followed by CCSM4 at 155 mm. NorESM1-M has the smallest $PIGL_{95}$ sea level contribution at 144 mm (Fig. 7). With increased γ_0, GCM dependence becomes more dependent on ocean forcing, as surface mass balance forcing is the same for experiments with the same GCM-scenario forcing. Increased sea level contribution for MIROC-ESM is partly driven by increases in EAIS mass loss (Fig. 9b e.g., sectors 4 (Queen Mary Land) and 5 (Totten sector) in Fig. 8) where thermal forcing is high (Fig. 1). Similarly, NorESM1-M undergoes large mass loss in EAIS where SMB is low whilst grounding line flux increases under high γ_0 (Fig. 9b). In WAIS, ocean thermal forcing drives a large grounding line flux under CCSM4 (Fig. 9a), particularly under high γ_0.

We also ran two simulations forced with a newer climate model (CMIP6) under newer emissions scenarios (SSPs). Comparing the CNRM-CM6-1, SSP5-8.5 with other high emission scenario CMIP5 forced experiments with $MeanAnt_{50}$, we see a lower sea level contribution at 2 mm. This is the lowest sea level contribution of any experiment. High SMB in all regions (Fig. 9c, d, f), whilst thermal forcing (Fig. 1) and grounding line flux are low (Fig. 9a, b, c) compared with other experiments result in less mass loss than other comparable experiments, or the control (Table 2).

3.6 Dependence on emissions scenario

The higher warming simulations (RCP8.5 for CMIP5 models and SSP5-8.5 for CMIP6) generally have higher SMB over the continent (Fig. 9) than low emissions scenario experiments, consistent with larger precipitation flux under warming (Payne

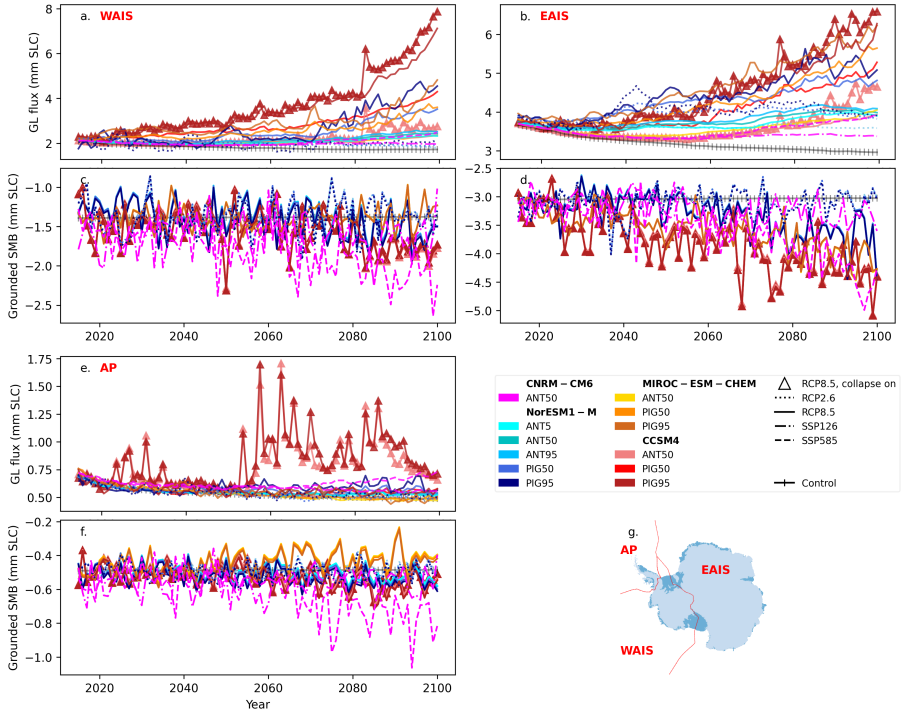

Figure 9. Total annual grounding line flux (mm SLC, positive values for mass loss) for the West Antarctic ice sheet (WAIS) (**a**), East Antarctic ice sheet (EAIS) (**b**) and the Antarctic Peninsula (AP) (**e**). Total annual grounded surface mass balance (mm SLC, so negative values indicate ice sheet mass gain) for WAIS (**c**), EAIS (**d**) and the AP (**f**). Region boundaries are also shown (**g**). Note that y-scales differ.

et al., 2021; Palerme et al., 2017; Frieler et al., 2015). The scenario dependence was then modulated by the value used for basal melt sensitivity.

Scenario-dependence was assessed for the two GCMs used to make projections under the low emissions scenarios (RCP2.6/SSP1-2.6): NorESM1-M from CMIP5 and CNRM-CM6-1 for CMIP6, calibrated to mean Antarctic melt rates. For the NorESM1-M simulations, the low emissions scenario leads to greater sea level contribution by 2100, i.e., counter to the intention of mitigating climate impacts: 91 mm under RCP2.6, compared with 84 mm under RCP8.5. This varies regionally: WAIS sea level contribution, for example, is smaller under RCP2.6 than RCP8.5 (47 mm vs 53 mm), as basal melting under RCP8.5 is greater (Fig. 9a), whilst SMB is lower under RCP2.6 (Fig. 9b). These factors together drive the higher mass loss in WAIS loss under RCP8.5 compared with RCP2.6 - consistent with other ISMIP6 ice sheet models forced by NorESM1-M, where mass loss is greater under RCP8.5 than RCP2.6 (Fig. 4a in Edwards et al. (2021)). For the EAIS and the majority of the Peninsula, the SMB scenario-dependence is reversed: SMB is higher under RCP8.5 compared with RCP2.6. This drives a smaller net sea level contribution in EAIS under RCP8.5 (29 mm vs 40 mm under RCP2.6), and in the Peninsula compared with RCP2.6 (4 mm vs 2 mm under RCP8.5), which is consistent with most other ISMIP6 models (Fig. 4c, d in Edwards et al. (2021)).

Simulations forced by the CMIP6 model CNRM-CM6-1 project low sea level contribution under both emissions scenarios: 2 mm under SSP5-8.5 and 53 mm under SSP1-2.6. WAIS, EAIS and AP all have less mass loss under SSP5-8.5 compared with SSP1-2.6. Unlike NorESM1-M, CNRM-CM6-1 consistently has higher SMB under the higher emissions scenario across the majority of the ice sheet (Fig. 9a, b, e). Basal melt is higher under the higher emissions scenario for CNRM-CM6-1 (Fig. 9c, d, f), though not by enough to counteract the SMB increases, so sea level contribution is smaller for all sectors (WAIS: 25 mm vs 15 mm, EAIS: 9 mm vs -10 mm, AP: 1 mm vs -3 mm). This is consistent with other ISMIP6 projections forced with this climate model, where accumulation under higher emissions exceeds ocean melt-driven mass loss (Fig. 4 in Edwards et al. (2021)).

Two additional simulations beyond the ISMIP6 protocol (T71 and T73) were run to provide insight into the modulation of scenario-dependence by basal melt sensitivity. These apply NorESM1-M thermal forcing under RCP2.6 with $PIGL_{50}$ and $PIGL_{95}$ basal melt sensitivity parameters. For the AP and EAIS, sea level contribution is comparable under both scenarios and γ_0 values (supplementary Table 1), indicating limited scenario dependence under $PIGL_{50}$ and $PIGL_{95}$ for NorESM1-M. In WAIS, sea level contribution increases by 33 mm and 34 mm under $PIGL_{50}$ and $PIGL_{95}$ respectively (supplementary Table 1). Under the Ross ice shelf, thermal forcing increases more under RCP8.5 compared with RCP2.6, than under Filchner-Ronne. For $PIGL_{50}$, RCP8.5 increases sea level contribution by 28 mm in the Ross sea sector, from -15 mm sea level contribution under RCP2.6 (Fig. 8-8, supplementary Table 1). Conversely, the Filchner-Ronne sector gains mass under both RCP8.5 (-15 mm SLC) and RCP 2.6 (-9 mm SLC) under $PIGL_{50}$. This demonstrates greater scenario dependence in the Ross sector compared with Filchner-Ronne. These experiments informed the assessment of potential interactions between scenario and basal melt sensitivity (see Contributions to Edwards et al. (2021) below).

For both scenario dependence, and GCM dependence, climate model sensitivity plays a significant role. CNRM-CM6-1 has an equilibrium climate sensitivity (ECS) of 4.8°C (Meehl et al., 2020), similar to MIROC-ESM-CHEM (ECS = 4.7°C) the highest ECS CMIP5 model sampled in ISMIP6 and discussed in Payne et al. (Payne et al. 2021), but higher than the remaining CMIP5 models which have ECS of 2.9°C (CCSM4) and 2.9°C (NorESM1-M)(Flato et al., 2013). This drove large positive surface mass balance and accumulation in CNRM-CM6-1, compared with the low emissions scenario simulation (Fig. 9). This offset dynamical losses from ocean melt-driven retreat.

3.7 Dependence on ice shelf collapse

Two pairs of simulations explore the impact of shelf collapse on sea level contribution. All are forced with the CCSM4 climate model under RCP8.5. The first pair have ice shelf collapse on and off, with the $MeanAnt_{50}$ basal melt parameter value (experiment 12 and 8, respectively). The second pair is the same but with the $PIGL_{95}$ parameter value (experiment TD58 and D58), to explore the interactions between the basal melt parameter and shelf collapse. Experiment TD58 was beyond the ISMIP6 protocol, and was performed to inform the synthesis by Edwards et al. (2021)

Including shelf collapse increases Antarctic sea level contribution by around 25 mm relative to 'no collapse' in both pairs of experiments (by region, the increase is: Peninsula: 13 mm; EAIS: 5-6 mm; WAIS 5-6 mm). However, the no collapse baseline is very different in the two basal melt parameterisations (8 mm sea level contribution under $MeanAnt_{50}$ compared with 155

mm under $PIGL_{95}$). These two sets of projections informed the assessment of interactions between ice shelf collapse and basal melt sensitivity (see Contributions to Edwards et al. (2021) below).

3.8 Dependence on basal melt sensitivity

To understand dependence of the projections on the basal melt parameter, experiments with the same GCM forcing and different γ_0 can be compared. Here all simulations have ice shelf collapse off. The most comprehensively sampled combination of GCM and scenario is NorESM1-M under RCP8.5: simulations were carried out for five basal melt sensitivity values, $MeanAnt_5$, $MeanAnt_{50}$, $MeanAnt_{95}$, $PIGL_{50}$ and $PIGL_{95}$. Three of these values ($MeanAnt_{50}$, $PIGL_{50}$ and $PIGL_{95}$), which span most of the range, were carried out also for NorESM1-M under RCP2.6, and for MIROC-ESM and CCSM4 under RCP8.5.

The overall γ_0-dependence for the majority of GCMs is one of increased sea level contribution under higher γ_0, as discussed throughout the results, though the nature of this relationship varies by region and model (Fig. 10). The Antarctic Peninsula is fairly insensitive to increases in γ_0 (Fig. 10c). In comparison with other ISMIP6 models, BISICLES has intermediate sensitivity to γ_0 (see Extended Data Fig. 6 in Edwards et al. 2021).

In the NorESM1-M experiments, increasing γ_0 from $PIGL_{50}$ to $PIGL_{95}$ leads to a more complex response in WAIS and EAIS than the simple increase in sea level contribution seen for other GCMs (Fig. 10a and b). Under RCP2.6, the $PIGL_{95}$ simulation counter intuitively undergoes a smaller loss of VAF than the $PIGL_{50}$ simulation (Fig. 4: darker blue dashed lines). Whilst localised thickening occurs intermittently for all GCMs and scenarios under $PIGL$ basal melt tuning (not shown), for NorESM1-M, thickening is pervasive enough to alter the dependence of net mass loss on γ_0. As can be seen in supplementary Figures 5k and l, the Ross ice shelf thickens in both simulations, with more thickening under $PIGL_{95}$. Under RCP8.5, the $PIGL_{95}$ simulation also projects smaller contribution to sea level than $PIGL_{50}$ for most of the century, until overtaking in 2094 (Fig. 4: blue solid lines) for the whole ice sheet.

4 Discussion

4.1 Basal melt sensitivity

In terms of basal melt sensitivity, previous studies using ISMIP6 non-local basal melt parameterisation have also noted ice shelf thickening as a result of refreezing under high γ_0 values (Lowry et al., 2021; Lipscomb et al., 2021). Ice shelf refreezing under low thermal forcing is plausible, and present in observations and model simulations of Antarctic ice shelf cavities (Naughten et al., 2018; Adusumilli et al., 2020; Reese et al., 2018; Stevens et al., 2020). However, Lipscomb et al. (2021) modify the second term in equation 1 to avoid what they suggest is spurious melting and refreezing where $\langle TF \rangle_{draft \in sector} + \delta T_{sector}$ is negative. An earlier study exploring Antarctic sensitivity to future climate and model parameters used an alternative basal melt approach that also avoids refreezing of ice shelves by design (Bulthuis et al., 2019).

Our BISICLES version uses the ISMIP6 non-local melt parameterisation without modification (Jourdain et al., 2020). However, thickening of ice shelves as a result of the basal melt parameterisation is not permitted in this BISICLES_B configuration.

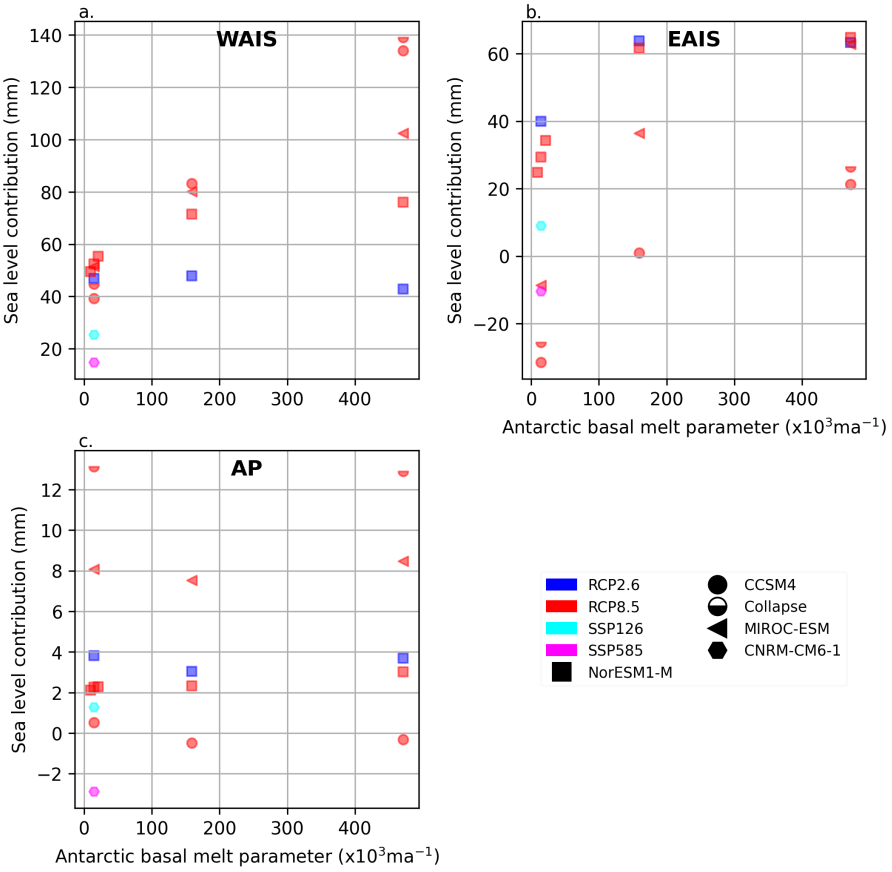

Figure 10. Sea level contribution from 2015 to 2100 for all simulations as a function of basal melt sensitivity (γ_0), shown for West Antarctic (WAIS) (**a**) East Antarctic (EAIS) **b**, and Peninsula (AP) **c** ice sheets.

Thickening of ice shelves under the highest γ_0 values could therefore be a manifestation of tributary glaciers responding to strong ice shelf thinning and removal of buttressing, and advection of ice to grounding lines as ice streams speed up. Beyond 100 year time scales, initial thickening could therefore precede a larger long-term sea level response. Future work could explore whether melt sensitivity dependence for highest γ_0 values reverts to that seen for lower values (higher γ_0, more mass loss) over longer time scales.

The Ross sector provides an example of an ice shelf and grounding line dynamic under $PIGL$ γ_0 tuning that runs counter to our expectation: that higher γ_0 will increase shelf thinning, and enhance grounding line retreat. For this and other sectors under NorESM1-M RCP2.6 and RCP8.5 (e.g. Sector 4: Totten, and Sector 5: George V), sea level rise contribution under the highest basal melt sensitivity ($PIGL_{95}$) is lower than under the second highest ($PIGL_{50}$) basal melt sensitivity (Fig. 8: blue solid lines). Figure 11a shows a transect through the grounding line at the terminus of Whillans and Mercer ice streams for $PIGL_{95}$ NorESM1-M RCP8.5 and $PIGL_{50}$ at three successive time slices (2015, 2050 and 2100). Also shown are the basin average

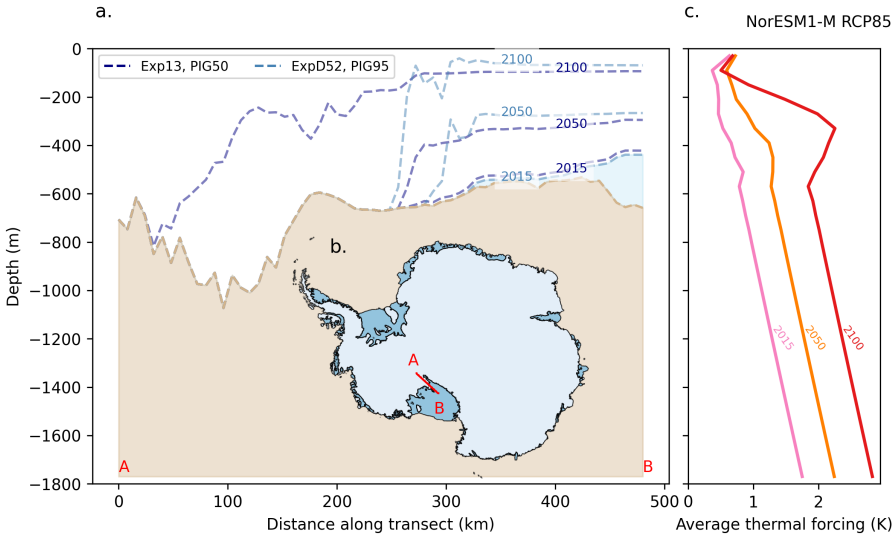

Figure 11. Subplot **a** shows a transect through the Siple coast for $PIGL_{50}$ (darker blue lines) and $PIGL_{95}$ (lighter blue lines) experiments under NorESM1-M RCP8.5. Blue dashed lines show ice sheet base for years indicated. Subplot **b** shows average thermal forcing with depth at successive time steps. Subplot **c** shows the transect location. The higher basal melt sensitivity (γ_0) run undergoes more thinning in outer shelf shown in transect, but grounding line retreats further inland for lower γ_0 run - though the shelf remains thicker for the latter.

thermal forcing for NorESM1-M RCP8.5 (Fig. 11c). In the Ross Sea Sector, the grounding line under $PIGL_{95}$ is seaward of the equivalent $PIGL_{50}$ simulation grounding line for the duration of the simulation at the Whillans and Mercer ice streams grounding line (Fig. 11a). Ross sector ice streams drain around 40% of the West Antarctic ice sheet (Price et al., 2001), so changes to ice stream configuration along the Siple coast impact sea level contribution in the sector.

4.2 Comparison with other models

To explore differences between BISICLES and ISMIP6 contributions from other models, we first compare control simulations. As noted in Seroussi et al. (2020), models employing a data assimilation approach to initialisation have larger mass trends through the control simulation. Seroussi et al. (2020) Table B2 presents total ice mass change, mass above floatation change, total area change and floating area change for ISMIP6 control experiments. BISICLES undergoes a total mass change of -50,149 Gt and a mass above floatation change of -19,220 Gt between 2015 and 2100 in the control experiment. The magnitude of mass change for both total mass and mass above floatation is comparable to other models using a data assimilation type initialisation. Total area change in our control is -6.9 x10^3 km^2 - with any area loss associated with regions of the ice sheet where decreases in thickness to 1 m result in calving. Floating area increases by 6.46 x10^4 km^2, consistent with regional grounding line retreat described in Section 3.1. Average annual basal melt is 2,139 Gt yr^{-1} for our control simulation, and integrated surface mass balance is 2,144 Gt yr^{-1}. This relatively low surface mass balance and high basal melting, combined

with our data assimilation type initialisation, likely contribute to BISICLES having the fourth highest mass loss in the control amongst ISMIP6 models ((Seroussi et al., 2020), Table B2).

We next compare BISICLES projections with other ISMIP6 models, and analyse regional contributions for experiments discussed in the main text - shown in Fig. 12. For the purpose of this comparison we subtract the control from our simulations, in line with the previous ISMIP6 results (Seroussi et al., 2020).

For the EAIS, BISICLES has the largest sea level contribution under mean Antarctic γ_0 tuning for NorESM1-M RCP8.5 forced simulations (Fig. 12a-d). With the largest EAIS contribution in these experiments sourced from the Totten Glacier, this could suggest that BISICLES 1 km grid resolution at the Totten grounding line is resolving retreat not captured in lower resolution models (4-20 km for fixed resolution models; minimum 2 km for variable resolution models) - though we note that Totten glacier can retreat at lower resolution (< 8 km) in BISICLES (Cornford et al., 2016). Previous studies have also highlighted that models using sub-grid interpolation schemes at the grounding line are more sensitive to forcing than conventional models (Tsai et al., 2015).

For WAIS (Fig. 12e-k), BISICLES projections for the core experiments tend to be mid-range and similar to two models with structural similarities: CISM, which is the other L1L2 physics model (though run on a fixed 4 km grid), and UCI JPL ISSM, which also uses a variable mesh resolution. CISM additionally implements a sub-grid interpolation scheme to represent basal melt in partially floating cells (Lipscomb et al., 2021), which could account for its slightly larger sea level contribution under NorESM1-M RCP8.5 core experiments for WAIS compared with BISICLES, which does not implement a sub-grid interpolation scheme for basal melting (Seroussi and Morlighem, 2018). Under increased basal melt sensitivity (γ_0), the CISM WAIS contribution is larger still. UCI JPL ISSM uses a variable mesh with finest resolution of 3 km near the margins, and has higher order physics (Seroussi et al., 2020). Agreement between ISSM and BISICLES for core WAIS simulations could reflect high resolution in both models, compared with other ISMIP6 models. We note that in the Marine Ice Sheet Model Intercomparison Project (MISMIP+), model physics had a less significant impact on simulated dynamics than basal sliding law, which is based on Weertman sliding for both BISICLES and UCI JPL ISSM, at comparable resolution (Cornford et al., 2020). Whilst BISICLES and ISSM have Weertman sliding over much of the domain, BISICLES uses a Tsai et al. (2015) type sliding law with Coulomb sliding close to the grounding line. This difference could be a factor where higher sea level contributions are simulated in BISICLES. The mm-scale magnitude of this difference is comparable to that found in previous studies comparing Weertman-only and Tsai et al. (2015) type sliding laws (Nias et al., 2018; Barnes and Gudmundsson, 2022).

4.3 Contributions to Edwards et al. (2021)

Simulations presented here were included in the synthesis of projections of global land ice contribution to 2100 sea level by Edwards et al. (2021), extending the ISMIP6 ensemble by an additional model compared with Seroussi et al. (2020) and Payne et al. (2021). Experiments beyond the main ISMIP6 protocol were also conducted to provide further exploration of sensitivities and interactions.

As outlined in Section 3.7, the increase in sea level with collapse on is almost identical for both basal melt sensitivities sampled ($MeanAnt_{50}$ and $PIGL_{95}$). Along with results from the same experiments in ISSM, this is the basis for the conclusion

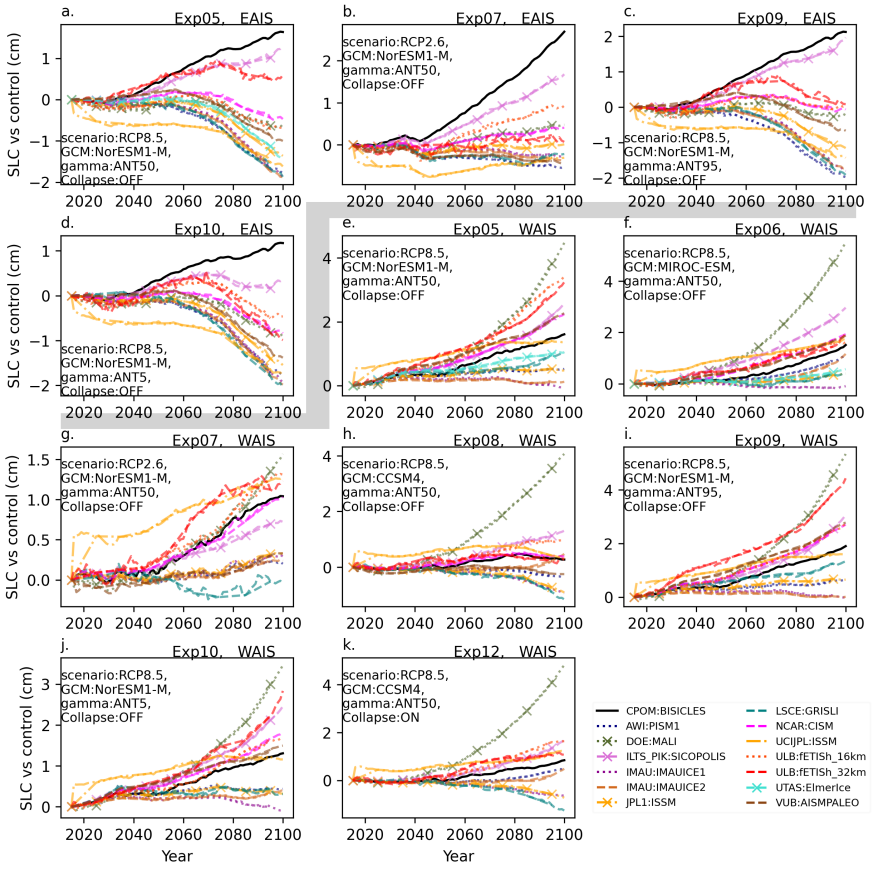

Figure 12. Comparison between BISICLES projections minus the control and other ISMIP6 models for experiments mentioned in the main text. Subplots above the grey divider (**a-d**) are for the East Antarctic Ice Sheet (EAIS) contribution for core experiments. Subplots below the grey divider (**e-k**) are for the West Antarctic Ice Sheet (WAIS) contribution for core experiments. Data from Edwards et al. (2021).

in Edwards et al. (2021, section "Ice shelf collapse versus basal melt") that contribution due to ice shelf collapse does not significantly increase with higher values of γ_0.

Sampling $PIGL$ basal melt sensitivity under RCP2.6 (T71 and T73) to compare with RCP8.5 projections shows that the spread of projections is smaller under RCP2.6, confirmed in complementary experiments with ISSM, as presented in Edwards et al. (2021, Section "Retreat and basal melt versus temperature").

4.4 Limitations

For NorESM1-M RCP2.6 $PIGL_{95}$, the sea level contribution until 2100 is lower than that projected under $PIGL_{50}$. However, the trajectory of mass loss in Figure 4 indicates that $PIGL_{95}$ could overtake $PIGL_{50}$ beyond 2100. Work is ongoing to extend these simulations to 2300, and will shed valuable light on mass loss under high basal melt sensitivity beyond 2100. More

broadly, IPCC AR6 extrapolates mass trends from 2100, the end of the simulation period for the model inter-comparisons it draws on, to project sea level to 2150 - a time horizon that is increasingly policy relevant for long-lived infrastructure (Fox-Kemper et al., 2021). With ice sheet model simulations beyond 2100, longer-term sea level projections should be informed by physics-based models, without the need to assume mass trends.

Another informative extension on the work presented here would be to more comprehensively explore model uncertainties. We explored five of the six γ_0 values provided by ISMIP6, omitting an intermediate ($PIGL_5$) values from our experiments. Future simulations could include this γ_0 value. Moreover, whilst we were limited to the discrete γ_0 values provided by ISMIP6, as calculating intermediate values was beyond the scope of this work, it is in practice a continuous parameter and additional values could be tested. Similarly, we did not explore the full range of boundary conditions provided by ISMIP6, or all possible combinations of uncertainties. With BISICLES a computationally expensive model and limited resources, a comprehensive uncertainty quantification was beyond the scope of the present study. However, future work could more systematically quantify uncertainties in GCM forcing, γ_0 values and parameter interactions in a comprehensive ensemble design, such as a Latin Hypercube. We note that recent studies find the $PIGL$ tuning of the ISMIP6 parameterisation leads to greater error, relative to an ocean model, in yearly integrated melt than $MeanAnt$ (Burgard et al., 2022). More broadly, we only explored the ISMIP6 non-local basal melt parameterisation. Burgard et al. (Burgard et al., 2022) explore a range of basal melt parameterisations, including the non-local ISMIP6 parameterisation used here, highlighting the importance of diverse basal melt parameterisations for modelling future ice sheet change.

We do not vary our basal sliding parameters, or explore different basal sliding parameterisations. Recent work suggests that different basal sliding laws and parameterisations drive broadly similar mass loss on decadal to century timescales (Barnes and Gudmundsson, 2022). However, previous work with BISICLES (Nias et al., 2018) suggests that a Coulomb sliding law leads to higher sea level contribution compared with Weertman sliding, whilst higher values of the exponent in the Weertman sliding law increase sea level contribution. Moreover, accounting for basal hydrology has the potential to increase century scale sea level contribution under ISMIP6 forcing compared with Weertman sliding (Kazmierczak et al., 2022). A comprehensive exploration of how basal sliding is represented would be an improvement on the work presented here.

As outlined in section 2.1, we used a fixed ice front except in experiments with ice shelf collapse. Given the importance of calving in reducing buttressing to grounded Antarctic ice, with mass loss from calving approximately equalling that from ice shelf thinning between 1997 and 2021 (Greene et al., 2022), failing to account for this likely under-predicts modelled sea level contribution (Haseloff and Sergienko, 2018). Future work should aim to incorporate a comprehensive calving model.

Ice sheet initial condition plays an important role in model uncertainty (Seroussi et al., 2019). However, exploring initial condition uncertainty was beyond the scope of this study. Future work could explore how consistent the BISICLES response to future climate and parameter uncertainty is, when the simulations begin from a different modern initial condition - such as one based on BedMachine (Morlighem et al., 2020) or Bedmap3 (Frémand et al., 2023).

The impacts of solid earth changes on projected ice sheet contribution to sea level are not explored for ISMIP6 (Nowicki et al., 2016), and we do not include them in our experiments. Some projection studies have incorporated simplified models of ice sheet bedrock interactions (Coulon et al., 2021; DeConto and Pollard, 2016; DeConto et al., 2021; Bulthuis et al.,

2019; Kachuck et al., 2020). Fast-responding, low viscosity mantle under West Antarctica, and elastic bedrock uplift can limit grounding line retreat (Larour et al., 2019; Kachuck et al., 2020). Conversely, bedrock uplift as marine ice sheets retreat can reduce accommodation space for ocean water, and therefore increase GMSL (Pan et al., 2021; Yousefi et al., 2022). The importance of bedrock processes in Antarctic response to anthropogenic climate change should be explored in future work.

5 Conclusions

We present projections of the Antarctic ice sheet over the coming century, performed with the BISICLES model for experiments based on the ISMIP6 protocol. We explored regional and sectoral ice sheet changes under a range of GCMs, low (RCP2.6, SSP1.26) and high (RCP8.5, SSP5.85) emissions scenarios, sensitivity to basal melt forcing and the role of ice shelf collapse. We also compared our results to those of other models that contributed to the ISMIP6 ensemble.

Climate model dependence in our ensemble is a result of high surface mass balance in some models offsetting dynamic losses, particularly under low γ_0 values. For example, CNRM-CM6-1, CCSM4 and MIROC-ESM have high surface mass balance over EAIS under the high emissions scenario, leading them to gain mass when γ_0 is low. Moreover, CNRM-CM6-1 has high surface mass balance over WAIS, so that it loses less mass than the control here under both emissions scenarios with $MeanAnt_{50}$ basal melt sensitivity. Conversely, low accumulation in NorESM1-M compared with other models contributes to relatively high regional sea level contribution for the EAIS. This highlights the important role increased EAIS mass gain under warming could play in offsetting dynamic mass loss, as highlighted in previous studies (Jordan et al., 2023; Stokes et al., 2022). It also shows, however, that projected sea level contribution is highly dependent on GCM and where it distributes accumulation and ocean melting around Antarctica. Determining which models produce more plausible warmer-than-modern Antarctic climates would improve confidence in future Antarctic mass projections.

The response to emissions scenario, i.e., global warming, is again strongly modulated by basal melt sensitivity (γ_0). Under very high emissions scenarios (RCP8.5, SSP5.85), if γ_0 is tuned to high melt rates (*PIGL*) then strong basal melt drives dynamic loss and large sea level contributions - despite increased surface mass balance under these scenarios. However, if basal melt sensitivity is low, increased snowfall accumulation under the warmer scenario, particularly over the EAIS, offsets dynamic mass loss. This leads to a more limited sea level contribution compared with RCP2.6 or SSP1.26.

Basal melt sensitivity plays a key role in determining both GCM dependence and emissions scenario sensitivity. It moderates the balance between accumulation-driven sea level fall on the one hand, and ocean melt-driven dynamical mass loss on the other. The role of γ_0 in balancing these processes, highlights the importance of constraining plausible values of basal melt sensitivity for Antarctica under future warming. Better characterisation of the relationship between thermal forcing and ice shelf melting, is key to more robust projections of future Antarctic sea level contribution.

Finally, ice shelf collapse increased sea level contribution overall in our simulations, highlighting the importance of calving in removing buttressing. It has a comparable effect on sea level contribution for both basal melt sensitivity values tested ($MeanAnt_{50}$ and $PIGL_{50}$). Based on the temperature-melt relationship proposed in Trusel et al. (2015), and a conservative interpretation of the limit of stability for ice shelves, under CCSM4 temperatures, we show that ice shelf collapse can contribute

to ~25 mm to sea level by 2100. Beyond 2100, surface warming-driven ice shelf collapse could become increasingly important for Antarctic stability. Ice shelf collapse could drive higher long-term Antarctic sea level contribution, regardless of basal melt sensitivity to ocean forcing.

Code and data availability. Code to reproduce analysis and figures is available on github https://github.com/jone006/imsip6_bisicles_paper. BISICLES model code is available on https://anag-repo.lbl.gov/svn/BISICLES/public/branches/ISMIP6-AIS/code/. BISICLES results data is available at 10.5281/zenodo.13880450

Author contributions. S.N lead the overall ISMIP6 project, and H.S. coordinated the Antarctic projections for ISMIP6. T.E developed additional experiments based on the ISMIP6 protocol, and formulated this study along with J.O.

D.M and C.S conducted core ISMIP6 experiments, J.O conducted non-core experiments and those outside the ISMIP6 protocol. C.S, D.M and S.C developed software for processing model outputs. J.O developed software to analyse and visualise all results presented in this paper. S.C and D.M were lead developers of the BISICLES ice sheet model, and developed the model set-up used for these experiments. D.M provided access to the National Energy Research Scientific Computing Center (NERSC) on which experiments were conducted, and storage access.

J.O wrote the first draft, all authors provided feedback and edits to improve the manuscript.

Competing interests. The authors declare that they have no competing interests

Acknowledgements. James O'Neill acknowledges support from the UK Natural Environment Research Council (NERC) (grant NE/L002485/1).

Support for this work was provided through the Scientific Discovery through Advanced Computing (SciDAC) program funded by the U.S. Department of Energy (DOE), Office of Science, Biological and Environmental Research and Advanced Scientific Computing Research programs, as a part of the ProSPect SciDAC Partnership. Work at Berkeley Lab was supported by the Director, Office of Science, of the U.S. Department of Energy under Contract No. DE-AC02-05CH11231. This research used resources of the National Energy Research Scientific Computing Center (NERSC), a U.S. Department of Energy Office of Science User Facility located at Lawrence Berkeley National Laboratory, operated under Contract No. DE-AC02-05CH11231 using NERSC award ASCR-ERCAPm1041. H.S. was supported by grants from the NASA Cryopsheric Science Program (#80NSSC21K1939 and #80NSSC22K0383). L.J.G. was funded by a UKRI Future Leaders Fellowship (MR/S016961/1). We thank the Climate and Cryosphere (CliC) effort, which provided support for ISMIP6 through sponsoring of workshops, hosting the ISMIP6 website and wiki, and promoted ISMIP6. We acknowledge the World Climate Research Programme, which, through its Working Group on Coupled Modelling, coordinated and promoted CMIP5 and CMIP6. We thank the climate modeling groups for producing and making available their model output, the Earth System Grid Federation (ESGF) for archiving the CMIP data and providing access, the University at Buffalo for ISMIP6 data distribution and upload, and the multiple funding agencies who support CMIP5

and CMIP6 and ESGF. We thank the ISMIP6 steering committee, the ISMIP6 model selection group and ISMIP6 dataset preparation group for their continuous engagement in defining ISMIP6. This is ISMIP6 contribution No 34.

References

Adusumilli, S., Fricker, H. A., Medley, B., Padman, L., and Siegfried, M. R.: Interannual variations in meltwater input to the Southern Ocean from Antarctic ice shelves, Nature Geoscience, 13, 616–620, https://doi.org/10.1038/s41561-020-0616-z, 2020.

Arthern, R. J., Winebrenner, D. P., and Vaughan, D. G.: Antarctic snow accumulation mapped using polarization of 4.3-cm wavelength microwave emission, Journal of Geophysical Research: Atmospheres, 111, https://doi.org/10.1029/2004JD005667, 2006.

Barnes, J. M. and Gudmundsson, G. H.: The predictive power of ice sheet models and the regional sensitivity of ice loss to basal sliding parameterisations: a case study of Pine Island and Thwaites glaciers, West Antarctica, The Cryosphere, 16, 4291–4304, https://doi.org/10.5194/tc-16-4291-2022, 2022.

Barthel, A., Agosta, C., Little, C. M., Hattermann, T., Jourdain, N. C., Goelzer, H., Nowicki, S., Seroussi, H., Straneo, F., and Bracegirdle, T. J.: CMIP5 model selection for ISMIP6 ice sheet model forcing: Greenland and Antarctica, The Cryosphere, 14, 855–879, https://doi.org/10.5194/tc-14-855-2020, 2020.

Bindschadler, R. A., Nowicki, S., Abe-Ouchi, A., Aschwanden, A., Choi, H., Fastook, J., Granzow, G., Greve, R., Gutowski, G., Herzfeld, U., Jackson, C., Johnson, J., Khroulev, C., Levermann, A., Lipscomb, W. H., Martin, M. A., Morlighem, M., Parizek, B. R., Pollard, D., Price, S. F., Ren, D., Saito, F., Sato, T., Seddik, H., Seroussi, H., Takahashi, K., Walker, R., and Wang, W. L.: Ice-sheet model sensitivities to environmental forcing and their use in projecting future sea level (the SeaRISE project), Journal of Glaciology, 59, 195–224, https://doi.org/10.3189/2013JoG12J125, 2013.

Bulthuis, K., Arnst, M., Sun, S., and Pattyn, F.: Uncertainty quantification of the multi-centennial response of the Antarctic ice sheet to climate change, The Cryosphere, 13, 1349–1380, https://doi.org/10.5194/tc-13-1349-2019, 2019.

Burgard, C., Jourdain, N. C., Reese, R., Jenkins, A., and Mathiot, P.: An assessment of basal melt parameterisations for Antarctic ice shelves, The Cryosphere, 16, 4931–4975, https://doi.org/10.5194/tc-16-4931-2022, 2022.

Cornford, S. L., Martin, D. F., Graves, D. T., Ranken, D. F., Le Brocq, A. M., Gladstone, R. M., Payne, A. J., Ng, E. G., and Lipscomb, W. H.: Adaptive mesh, finite volume modeling of marine ice sheets, Journal of Computational Physics, 232, 529–549, https://doi.org/10.1016/j.jcp.2012.08.037, 2013.

Cornford, S. L., Martin, D. F., Payne, A. J., Ng, E. G., Le Brocq, A. M., Gladstone, R. M., Edwards, T. L., Shannon, S. R., Agosta, C., van den Broeke, M. R., Hellmer, H. H., Krinner, G., Ligtenberg, S. R. M., Timmermann, R., and Vaughan, D. G.: Century-scale simulations of the response of the West Antarctic Ice Sheet to a warming climate, The Cryosphere, 9, 1579–1600, https://doi.org/10.5194/tc-9-1579-2015, 2015.

Cornford, S. L., Martin, D. F., Lee, V., Payne, A. J., and Ng, E. G.: Adaptive mesh refinement versus subgrid friction interpolation in simulations of Antarctic ice dynamics, Annals of Glaciology, 57, 1–9, https://doi.org/10.1017/aog.2016.13, 2016.

Cornford, S. L., Seroussi, H., Asay-Davis, X. S., Gudmundsson, G. H., Arthern, R., Borstad, C., Christmann, J., Dias dos Santos, T., Feldmann, J., Goldberg, D., Hoffman, M. J., Humbert, A., Kleiner, T., Leguy, G., Lipscomb, W. H., Merino, N., Durand, G., Morlighem, M., Pollard, D., Rückamp, M., Williams, C. R., and Yu, H.: Results of the third Marine Ice Sheet Model Intercomparison Project (MISMIP+), The Cryosphere, 14, 2283–2301, https://doi.org/10.5194/tc-14-2283-2020, 2020.

Coulon, V., Bulthuis, K., Whitehouse, P. L., Sun, S., Haubner, K., Zipf, L., and Pattyn, F.: Contrasting Response of West and East Antarctic Ice Sheets to Glacial Isostatic Adjustment, Journal of Geophysical Research: Earth Surface, 126, e2020JF006 003, https://doi.org/10.1029/2020JF006003, 2021.

Crawford, A. J., Benn, D. I., Todd, J., Åström, J. A., Bassis, J. N., and Zwinger, T.: Marine ice-cliff instability modeling shows mixed-mode ice-cliff failure and yields calving rate parameterization, Nature Communications, 12, 2701, https://doi.org/10.1038/s41467-021-23070-7, number: 1 Publisher: Nature Publishing Group, 2021.

DeConto, R. M. and Pollard, D.: Contribution of Antarctica to past and future sea-level rise, Nature, 531, 591–597, https://doi.org/10.1038/nature17145, 2016.

DeConto, R. M., Pollard, D., Alley, R. B., Velicogna, I., Gasson, E., Gomez, N., Sadai, S., Condron, A., Gilford, D. M., Ashe, E. L., Kopp, R. E., Li, D., and Dutton, A.: The Paris Climate Agreement and future sea-level rise from Antarctica, Nature, 593, 83–89, https://doi.org/10.1038/s41586-021-03427-0, 2021.

Depoorter, M. A., Bamber, J. L., Griggs, J. A., Lenaerts, J. T. M., Ligtenberg, S. R. M., van den Broeke, M. R., and Moholdt, G.: Calving fluxes and basal melt rates of Antarctic ice shelves, Nature, 502, 89–92, https://doi.org/10.1038/nature12567, 2013.

Edwards, T. L., Fettweis, X., Gagliardini, O., Gillet-Chaulet, F., Goelzer, H., Gregory, J. M., Hoffman, M., Huybrechts, P., Payne, A. J., Perego, M., Price, S., Quiquet, A., and Ritz, C.: Effect of uncertainty in surface mass balance–elevation feedback on projections of the future sea level contribution of the Greenland ice sheet, The Cryosphere, 8, 195–208, https://doi.org/10.5194/tc-8-195-2014, 2014.

Edwards, T. L., Brandon, M. A., Durand, G., Edwards, N. R., Golledge, N. R., Holden, P. B., Nias, I. J., Payne, A. J., Ritz, C., and Wernecke, A.: Revisiting Antarctic ice loss due to marine ice-cliff instability, Nature, 566, 58–64, https://doi.org/10.1038/s41586-019-0901-4, 2019.

Edwards, T. L., Nowicki, S., Marzeion, B., Hock, R., Goelzer, H., Seroussi, H., Jourdain, N. C., Slater, D. A., Turner, F. E., Smith, C. J., McKenna, C. M., Simon, E., Abe-Ouchi, A., Gregory, J. M., Larour, E., Lipscomb, W. H., Payne, A. J., Shepherd, A., Agosta, C., Alexander, P., Albrecht, T., Anderson, B., Asay-Davis, X., Aschwanden, A., Barthel, A., Bliss, A., Calov, R., Chambers, C., Champollion, N., Choi, Y., Cullather, R., Cuzzone, J., Dumas, C., Felikson, D., Fettweis, X., Fujita, K., Galton-Fenzi, B. K., Gladstone, R., Golledge, N. R., Greve, R., Hattermann, T., Hoffman, M. J., Humbert, A., Huss, M., Huybrechts, P., Immerzeel, W., Kleiner, T., Kraaijenbrink, P., Le clec'h, S., Lee, V., Leguy, G. R., Little, C. M., Lowry, D. P., Malles, J.-H., Martin, D. F., Maussion, F., Morlighem, M., O'Neill, J. F., Nias, I., Pattyn, F., Pelle, T., Price, S. F., Quiquet, A., Radić, V., Reese, R., Rounce, D. R., Rückamp, M., Sakai, A., Shafer, C., Schlegel, N.-J., Shannon, S., Smith, R. S., Straneo, F., Sun, S., Tarasov, L., Trusel, L. D., Van Breedam, J., van de Wal, R., van den Broeke, M., Winkelmann, R., Zekollari, H., Zhao, C., Zhang, T., and Zwinger, T.: Projected land ice contributions to twenty-first-century sea level rise, Nature, 593, 74–82, https://doi.org/10.1038/s41586-021-03302-y, 2021.

Favier, L., Jourdain, N. C., Jenkins, A., Merino, N., Durand, G., Gagliardini, O., Gillet-Chaulet, F., and Mathiot, P.: Assessment of sub-shelf melting parameterisations using the ocean–ice-sheet coupled model NEMO(v3.6)–Elmer/Ice(v8.3), Geoscientific Model Development, 12, 2255–2283, https://doi.org/10.5194/gmd-12-2255-2019, 2019.

Flato, G., Marotzke, J., Abiodun, B., Braconnot, P., Chou, S. C., Collins, W., Cox, P., Driouech, F., Emori, S., Eyring, V., Forest, C., Gleckler, P., Guilyardi, E., Jakob, C., Kattsov, V., Reason, C., and Rummukainen, M.: Evaluation of climate models, in: Climate Change 2013: The Physical Science Basis. Contribution of Working Group I to the Fifth Assessment Report of the Intergovernmental Panel on Climate Change, edited by Stocker, T. F., Qin, D., Plattner, G.-K., Tignor, M., Allen, S. K., Doschung, J., Nauels, A., Xia, Y., Bex, V., and Midgley, P. M., pp. 741–882, Cambridge University Press, Cambridge, UK, https://doi.org/10.1017/CBO9781107415324.020, 2013.

Fox-Kemper, B., Hewitt, H. T., Xiao, C., Aðalgeirsdóttir, G., Drijfhout, S. S., Edwards, T. L., Golledge, N. R., Hemer, M., Kopp, R. E., Krinner, G., Mix, A., Notz, D., Nowicki, S., Nurhati, I. S., Ruiz, L., Sallée, J.-B., Slangen, A. B. A., and Yu, Y.: Ocean, cryosphere, and sea level change, in: Climate Change 2021: The Physical Science Basis. Contribution of Working Group I to the Sixth Assessment Report of the Intergovernmental Panel on Climate Change, edited by Masson-Delmotte, V., Zhai, P., Pirani, A., Connors, S. L., Péan, C., Berger,

S., Caud, N., Chen, Y., Goldfarb, L., Gomis, M. I., Huang, M., Leitzell, K., Lonnoy, E., Matthews, J. B. R., Maycock, T. K., Waterfield, T., Yelekçi, , Yu, R., and Zhou, B., Cambridge University Press, 2021.

Frémand, A. C., Fretwell, P., Bodart, J. A., Pritchard, H. D., Aitken, A., Bamber, J. L., Bell, R., Bianchi, C., Bingham, R. G., Blankenship, D. D., Casassa, G., Catania, G., Christianson, K., Conway, H., Corr, H. F. J., Cui, X., Damaske, D., Damm, V., Drews, R., Eagles, G., Eisen, O., Eisermann, H., Ferraccioli, F., Field, E., Forsberg, R., Franke, S., Fujita, S., Gim, Y., Goel, V., Gogineni, S. P., Greenbaum, J., Hills, B., Hindmarsh, R. C. A., Hoffman, A. O., Holmlund, P., Holschuh, N., Holt, J. W., Horlings, A. N., Humbert, A., Jacobel, R. W., Jansen, D., Jenkins, A., Jokat, W., Jordan, T., King, E., Kohler, J., Krabill, W., Kusk Gillespie, M., Langley, K., Lee, J., Leitchenkov, G., Leuschen, C., Luyendyk, B., MacGregor, J., MacKie, E., Matsuoka, K., Morlighem, M., Mouginot, J., Nitsche, F. O., Nogi, Y., Nost, O. A., Paden, J., Pattyn, F., Popov, S. V., Rignot, E., Rippin, D. M., Rivera, A., Roberts, J., Ross, N., Ruppel, A., Schroeder, D. M., Siegert, M. J., Smith, A. M., Steinhage, D., Studinger, M., Sun, B., Tabacco, I., Tinto, K., Urbini, S., Vaughan, D., Welch, B. C., Wilson, D. S., Young, D. A., and Zirizzotti, A.: Antarctic Bedmap data: Findable, Accessible, Interoperable, and Reusable (FAIR) sharing of 60 years of ice bed, surface, and thickness data, Earth System Science Data, 15, 2695–2710, https://doi.org/10.5194/essd-15-2695-2023, 2023.

Frieler, K., Clark, P. U., He, F., Buizert, C., Reese, R., Ligtenberg, S. R. M., van den Broeke, M. R., Winkelmann, R., and Levermann, A.: Consistent evidence of increasing Antarctic accumulation with warming, Nature Climate Change, 5, 348–352, https://doi.org/10.1038/nclimate2574, 2015.

Goelzer, H., Coulon, V., Pattyn, F., de Boer, B., and van de Wal, R.: Brief communication: On calculating the sea-level contribution in marine ice-sheet models, The Cryosphere, 14, 833–840, https://doi.org/10.5194/tc-14-833-2020, publisher: Copernicus GmbH, 2020.

Golledge, N. R., Kowalewski, D. E., Naish, T. R., Levy, R. H., Fogwill, C. J., and Gasson, E. G. W.: The multi-millennial Antarctic commitment to future sea-level rise, Nature, 526, 421–425, https://doi.org/10.1038/nature15706, 2015.

Gong, Y., Cornford, S. L., and Payne, A. J.: Modelling the response of the Lambert Glacier–Amery Ice Shelf system, East Antarctica, to uncertain climate forcing over the 21st and 22nd centuries, The Cryosphere, 8, 1057–1068, https://doi.org/10.5194/tc-8-1057-2014, 2014.

Greene, C. A., Gardner, A. S., Schlegel, N.-J., and Fraser, A. D.: Antarctic calving loss rivals ice-shelf thinning, Nature, 609, 948–953, https://doi.org/10.1038/s41586-022-05037-w, 2022.

Gregory, J. M., Griffies, S. M., Hughes, C. W., Lowe, J. A., Church, J. A., Fukimori, I., Gomez, N., Kopp, R. E., Landerer, F., Cozannet, G. L., Ponte, R. M., Stammer, D., Tamisiea, M. E., and van de Wal, R. S. W.: Concepts and Terminology for Sea Level: Mean, Variability and Change, Both Local and Global, Surveys in Geophysics, 40, 1251–1289, https://doi.org/10.1007/s10712-019-09525-z, 2019.

Haseloff, M. and Sergienko, O. V.: The effect of buttressing on grounding line dynamics, Journal of Glaciology, 64, 417–431, https://doi.org/10.1017/jog.2018.30, 2018.

Holland, P. R., Bracegirdle, T. J., Dutrieux, P., Jenkins, A., and Steig, E. J.: West Antarctic ice loss influenced by internal climate variability and anthropogenic forcing, Nature Geoscience, 12, 718–724, https://doi.org/10.1038/s41561-019-0420-9, 2019.

Horwath, M., Gutknecht, B. D., Cazenave, A., Palanisamy, H. K., Marti, F., Marzeion, B., Paul, F., Le Bris, R., Hogg, A. E., Otosaka, I., Shepherd, A., Döll, P., Cáceres, D., Müller Schmied, H., Johannessen, J. A., Nilsen, J. E. , Raj, R. P., Forsberg, R., Sandberg Sørensen, L., Barletta, V. R., Simonsen, S. B., Knudsen, P., Andersen, O. B., Ranndal, H., Rose, S. K., Merchant, C. J., Macintosh, C. R., von Schuckmann, K., Novotny, K., Groh, A., Restano, M., and Benveniste, J.: Global sea-level budget and ocean-mass budget, with a focus on advanced data products and uncertainty characterisation, Earth System Science Data, 14, 411–447, https://doi.org/10.5194/essd-14-411-2022, 2022.

Jordan, J. R., Miles, B. W. J., Gudmundsson, G. H., Jamieson, S. S. R., Jenkins, A., and Stokes, C. R.: Increased warm water intrusions could cause mass loss in East Antarctica during the next 200 years, Nature Communications, 14, 1825, https://doi.org/10.1038/s41467-023-37553-2, 2023.

Jourdain, N. C., Mathiot, P., Merino, N., Durand, G., Le Sommer, J., Spence, P., Dutrieux, P., and Madec, G.: Ocean circulation and sea-ice thinning induced by melting ice shelves in the Amundsen Sea, Journal of Geophysical Research: Oceans, 122, 2550–2573, https://doi.org/10.1002/2016JC012509, 2017.

Jourdain, N. C., Asay-Davis, X., Hattermann, T., Straneo, F., Seroussi, H., Little, C. M., and Nowicki, S.: A protocol for calculating basal melt rates in the ISMIP6 Antarctic ice sheet projections, The Cryosphere, 14, 3111–3134, https://doi.org/10.5194/tc-14-3111-2020, 2020.

Kachuck, S. B., Martin, D. F., Bassis, J. N., and Price, S. F.: Rapid Viscoelastic Deformation Slows Marine Ice Sheet Instability at Pine Island Glacier, Geophysical Research Letters, 47, e2019GL086 446, https://doi.org/10.1029/2019GL086446, 2020.

Kazmierczak, E., Sun, S., Coulon, V., and Pattyn, F.: Subglacial hydrology modulates basal sliding response of the Antarctic ice sheet to climate forcing, The Cryosphere, 16, 4537–4552, https://doi.org/10.5194/tc-16-4537-2022, 2022.

Larour, E., Seroussi, H., Adhikari, S., Ivins, E., Caron, L., Morlighem, M., and Schlegel, N.: Slowdown in Antarctic mass loss from solid Earth and sea-level feedbacks, Science, https://doi.org/10.1126/science.aav7908, 2019.

Lipscomb, W. H., Leguy, G. R., Jourdain, N. C., Asay-Davis, X., Seroussi, H., and Nowicki, S.: ISMIP6-based projections of ocean-forced Antarctic Ice Sheet evolution using the Community Ice Sheet Model, The Cryosphere, 15, 633–661, https://doi.org/10.5194/tc-15-633-2021, 2021.

Lowry, D. P., Krapp, M., Golledge, N. R., and Alevropoulos-Borrill, A.: The influence of emissions scenarios on future Antarctic ice loss is unlikely to emerge this century, Communications Earth & Environment, 2, 1–14, https://doi.org/10.1038/s43247-021-00289-2, 2021.

Medley, B. and Thomas, E. R.: Increased snowfall over the Antarctic Ice Sheet mitigated twentieth-century sea-level rise, Nature Climate Change, 9, 34–39, https://doi.org/10.1038/s41558-018-0356-x, 2019.

Meehl, G. A., Senior, C. A., Eyring, V., Flato, G., Lamarque, J.-F., Stouffer, R. J., Taylor, K. E., and Schlund, M.: Context for interpreting equilibrium climate sensitivity and transient climate response from the CMIP6 Earth system models, Science Advances, 6, eaba1981, https://doi.org/10.1126/sciadv.aba1981, 2020.

Morlighem, M., Rignot, E., Binder, T., Blankenship, D., Drews, R., Eagles, G., Eisen, O., Ferraccioli, F., Forsberg, R., Fretwell, P., Goel, V., Greenbaum, J. S., Gudmundsson, H., Guo, J., Helm, V., Hofstede, C., Howat, I., Humbert, A., Jokat, W., Karlsson, N. B., Lee, W. S., Matsuoka, K., Millan, R., Mouginot, J., Paden, J., Pattyn, F., Roberts, J., Rosier, S., Ruppel, A., Seroussi, H., Smith, E. C., Steinhage, D., Sun, B., Broeke, M. R. v. d., Ommen, T. D. v., Wessem, M. v., and Young, D. A.: Deep glacial troughs and stabilizing ridges unveiled beneath the margins of the Antarctic ice sheet, Nature Geoscience, 13, 132–137, https://doi.org/10.1038/s41561-019-0510-8, 2020.

Morlighem, M., Goldberg, D., Barnes, J. M., Bassis, J. N., Benn, D. I., Crawford, A. J., Gudmundsson, G. H., and Seroussi, H.: The West Antarctic Ice Sheet may not be vulnerable to marine ice cliff instability during the 21st century, Science Advances, 10, eado7794, https://doi.org/10.1126/sciadv.ado7794, 2024.

Naughten, K. A., Meissner, K. J., Galton-Fenzi, B. K., England, M. H., Timmermann, R., Hellmer, H. H., Hattermann, T., and Debernard, J. B.: Intercomparison of Antarctic ice-shelf, ocean, and sea-ice interactions simulated by MetROMS-iceshelf and FESOM 1.4, Geoscientific Model Development, 11, 1257–1292, https://doi.org/10.5194/gmd-11-1257-2018, 2018.

Nias, I. J., Cornford, S. L., and Payne, A. J.: New Mass-Conserving Bedrock Topography for Pine Island Glacier Impacts Simulated Decadal Rates of Mass Loss, Geophysical Research Letters, 45, 3173–3181, https://doi.org/https://doi.org/10.1002/2017GL076493, 2018.

Nowicki, S., Goelzer, H., Seroussi, H., Payne, A. J., Lipscomb, W. H., Abe-Ouchi, A., Agosta, C., Alexander, P., Asay-Davis, X. S., Barthel, A., Bracegirdle, T. J., Cullather, R., Felikson, D., Fettweis, X., Gregory, J. M., Hattermann, T., Jourdain, N. C., Kuipers Munneke, P., Larour, E., Little, C. M., Morlighem, M., Nias, I., Shepherd, A., Simon, E., Slater, D., Smith, R. S., Straneo, F., Trusel, L. D., van den Broeke, M. R., and van de Wal, R.: Experimental protocol for sea level projections from ISMIP6 stand-alone ice sheet models, The Cryosphere, 14, 2331–2368, https://doi.org/10.5194/tc-14-2331-2020, 2020.

Nowicki, S. M. J., Payne, A., Larour, E., Seroussi, H., Goelzer, H., Lipscomb, W., Gregory, J., Abe-Ouchi, A., and Shepherd, A.: Ice Sheet Model Intercomparison Project (ISMIP6) contribution to CMIP6, Geoscientific Model Development, 9, 4521–4545, https://doi.org/10.5194/gmd-9-4521-2016, 2016.

Otosaka, I. N., Shepherd, A., Ivins, E. R., Schlegel, N.-J., Amory, C., van den Broeke, M. R., Horwath, M., Joughin, I., King, M. D., Krinner, G., Nowicki, S., Payne, A. J., Rignot, E., Scambos, T., Simon, K. M., Smith, B. E., Sørensen, L. S., Velicogna, I., Whitehouse, P. L., A, G., Agosta, C., Ahlstrøm, A. P., Blazquez, A., Colgan, W., Engdahl, M. E., Fettweis, X., Forsberg, R., Gallée, H., Gardner, A., Gilbert, L., Gourmelen, N., Groh, A., Gunter, B. C., Harig, C., Helm, V., Khan, S. A., Kittel, C., Konrad, H., Langen, P. L., Lecavalier, B. S., Liang, C.-C., Loomis, B. D., McMillan, M., Melini, D., Mernild, S. H., Mottram, R., Mouginot, J., Nilsson, J., Noël, B., Pattle, M. E., Peltier, W. R., Pie, N., Roca, M., Sasgen, I., Save, H. V., Seo, K.-W., Scheuchl, B., Schrama, E. J. O., Schröder, L., Simonsen, S. B., Slater, T., Spada, G., Sutterley, T. C., Vishwakarma, B. D., van Wessem, J. M., Wiese, D., van der Wal, W., and Wouters, B.: Mass balance of the Greenland and Antarctic ice sheets from 1992 to 2020, Earth System Science Data, 15, 1597–1616, https://doi.org/10.5194/essd-15-1597-2023, 2023.

Palerme, C., Genthon, C., Claud, C., Kay, J. E., Wood, N. B., and L'Ecuyer, T.: Evaluation of current and projected Antarctic precipitation in CMIP5 models, Climate Dynamics, 48, 225–239, https://doi.org/10.1007/s00382-016-3071-1, 2017.

Pan, L., Powell, E. M., Latychev, K., Mitrovica, J. X., Creveling, J. R., Gomez, N., Hoggard, M. J., and Clark, P. U.: Rapid postglacial rebound amplifies global sea level rise following West Antarctic Ice Sheet collapse, Science Advances, 7, eabf7787, https://doi.org/10.1126/sciadv.abf7787, 2021.

Pattyn, F.: Antarctic subglacial conditions inferred from a hybrid ice sheet/ice stream model, Earth and Planetary Science Letters, 295, 451–461, https://doi.org/10.1016/j.epsl.2010.04.025, 2010.

Pattyn, F., Favier, L., Sun, S., and Durand, G.: Progress in Numerical Modeling of Antarctic Ice-Sheet Dynamics, Current Climate Change Reports, 3, 174–184, https://doi.org/10.1007/s40641-017-0069-7, 2017.

Payne, A. J., Nowicki, S., Abe-Ouchi, A., Agosta, C., Alexander, P., Albrecht, T., Asay-Davis, X., Aschwanden, A., Barthel, A., Bracegirdle, T. J., Calov, R., Chambers, C., Choi, Y., Cullather, R., Cuzzone, J., Dumas, C., Edwards, T. L., Felikson, D., Fettweis, X., Galton-Fenzi, B. K., Goelzer, H., Gladstone, R., Golledge, N. R., Gregory, J. M., Greve, R., Hattermann, T., Hoffman, M. J., Humbert, A., Huybrechts, P., Jourdain, N. C., Kleiner, T., Munneke, P. K., Larour, E., Le clec'h, S., Lee, V., Leguy, G., Lipscomb, W. H., Little, C. M., Lowry, D. P., Morlighem, M., Nias, I., Pattyn, F., Pelle, T., Price, S. F., Quiquet, A., Reese, R., Rückamp, M., Schlegel, N.-J., Seroussi, H., Shepherd, A., Simon, E., Slater, D., Smith, R. S., Straneo, F., Sun, S., Tarasov, L., Trusel, L. D., Van Breedam, J., van de Wal, R., van den Broeke, M., Winkelmann, R., Zhao, C., Zhang, T., and Zwinger, T.: Future Sea Level Change Under Coupled Model Intercomparison Project Phase 5 and Phase 6 Scenarios From the Greenland and Antarctic Ice Sheets, Geophysical Research Letters, 48, e2020GL091 741, https://doi.org/10.1029/2020GL091741, 2021.

Pollard, D., DeConto, R. M., and Alley, R. B.: Potential Antarctic Ice Sheet retreat driven by hydrofracturing and ice cliff failure, Earth and Planetary Science Letters, 412, 112–121, https://doi.org/10.1016/j.epsl.2014.12.035, 2015.

Price, S. F., Bindschadler, R. A., Hulbe, C. L., and Joughin, I. R.: Post-stagnation behavior in the upstream regions of Ice Stream C, West Antarctica, Journal of Glaciology, 47, 283–294, https://doi.org/10.3189/172756501781832232, 2001.

Reese, R., Albrecht, T., Mengel, M., Asay-Davis, X., and Winkelmann, R.: Antarctic sub-shelf melt rates via PICO, The Cryosphere, 12, 1969–1985, https://doi.org/10.5194/tc-12-1969-2018, 2018.

Rignot, E., Jacobs, S., Mouginot, J., and Scheuchl, B.: Ice-Shelf Melting Around Antarctica, Science, 341, 266–270, https://doi.org/10.1126/science.1235798, 2013.

Rignot, E., Mouginot, J., Scheuchl, B., Broeke, M. v. d., Wessem, M. J. v., and Morlighem, M.: Four decades of Antarctic Ice Sheet mass balance from 1979–2017, Proceedings of the National Academy of Sciences, 116, 1095–1103, https://doi.org/10.1073/pnas.1812883116, 2019.

Ritz, C., Edwards, T. L., Durand, G., Payne, A. J., Peyaud, V., and Hindmarsh, R. C. A.: Potential sea-level rise from Antarctic ice-sheet instability constrained by observations, Nature, 528, 115–118, https://doi.org/10.1038/nature16147, 2015.

Robel, A. A., Seroussi, H., and Roe, G. H.: Marine ice sheet instability amplifies and skews uncertainty in projections of future sea-level rise, Proceedings of the National Academy of Sciences, 116, 14 887–14 892, https://doi.org/10.1073/pnas.1904822116, 2019.

Scambos, T., Fricker, H. A., Liu, C.-C., Bohlander, J., Fastook, J., Sargent, A., Massom, R., and Wu, A.-M.: Ice shelf disintegration by plate bending and hydro-fracture: Satellite observations and model results of the 2008 Wilkins ice shelf break-ups, Earth and Planetary Science Letters, 280, 51–60, https://doi.org/10.1016/j.epsl.2008.12.027, 2009.

Schlegel, N.-J., Seroussi, H., Schodlok, M. P., Larour, E. Y., Boening, C., Limonadi, D., Watkins, M. M., Morlighem, M., and van den Broeke, M. R.: Exploration of Antarctic Ice Sheet 100-year contribution to sea level rise and associated model uncertainties using the ISSM framework, The Cryosphere, 12, 3511–3534, https://doi.org/10.5194/tc-12-3511-2018, 2018.

Schoof, C.: Marine ice sheet stability, Journal of Fluid Mechanics, 698, 62–72, https://doi.org/10.1017/jfm.2012.43, 2012.

Seroussi, H. and Morlighem, M.: Representation of basal melting at the grounding line in ice flow models, The Cryosphere, 12, 3085–3096, https://doi.org/10.5194/tc-12-3085-2018, 2018.

Seroussi, H., Nowicki, S., Simon, E., Abe-Ouchi, A., Albrecht, T., Brondex, J., Cornford, S., Dumas, C., Gillet-Chaulet, F., Goelzer, H., Golledge, N. R., Gregory, J. M., Greve, R., Hoffman, M. J., Humbert, A., Huybrechts, P., Kleiner, T., Larour, E., Leguy, G., Lipscomb, W. H., Lowry, D., Mengel, M., Morlighem, M., Pattyn, F., Payne, A. J., Pollard, D., Price, S. F., Quiquet, A., Reerink, T. J., Reese, R., Rodehacke, C. B., Schlegel, N.-J., Shepherd, A., Sun, S., Sutter, J., Van Breedam, J., van de Wal, R. S. W., Winkelmann, R., and Zhang, T.: initMIP-Antarctica: an ice sheet model initialization experiment of ISMIP6, The Cryosphere, 13, 1441–1471, https://doi.org/10.5194/tc-13-1441-2019, 2019.

Seroussi, H., Nowicki, S., Payne, A. J., Goelzer, H., Lipscomb, W. H., Abe-Ouchi, A., Agosta, C., Albrecht, T., Asay-Davis, X., Barthel, A., Calov, R., Cullather, R., Dumas, C., Galton-Fenzi, B. K., Gladstone, R., Golledge, N. R., Gregory, J. M., Greve, R., Hattermann, T., Hoffman, M. J., Humbert, A., Huybrechts, P., Jourdain, N. C., Kleiner, T., Larour, E., Leguy, G. R., Lowry, D. P., Little, C. M., Morlighem, M., Pattyn, F., Pelle, T., Price, S. F., Quiquet, A., Reese, R., Schlegel, N.-J., Shepherd, A., Simon, E., Smith, R. S., Straneo, F., Sun, S., Trusel, L. D., Van Breedam, J., van de Wal, R. S. W., Winkelmann, R., Zhao, C., Zhang, T., and Zwinger, T.: ISMIP6 Antarctica: a multi-model ensemble of the Antarctic ice sheet evolution over the 21st century, The Cryosphere, 14, 3033–3070, https://doi.org/10.5194/tc-14-3033-2020, 2020.

Seroussi, H., Pelle, T., Lipscomb, W. H., Abe-Ouchi, A., Albrecht, T., Alvarez-Solas, J., Asay-Davis, X., Barre, J.-B., Berends, C. J., Bernales, J., Blasco, J., Caillet, J., Chandler, D. M., Coulon, V., Cullather, R., Dumas, C., Galton-Fenzi, B. K., Garbe, J., Gillet-Chaulet, F., Gladstone, R., Goelzer, H., Golledge, N., Greve, R., Gudmundsson, G. H., Han, H. K., Hillebrand, T. R., Hoffman, M. J., Huybrechts, P., Jourdain, N. C., Klose, A. K., Langebroek, P. M., Leguy, G. R., Lowry, D. P., Mathiot, P., Montoya, M., Morlighem, M., Nowicki, S., Pattyn, F., Payne, A. J., Quiquet, A., Reese, R., Robinson, A., Saraste, L., Simon, E. G., Sun, S., Twarog, J. P., Trusel, L. D., Urruty, B.,

Van Breedam, J., van de Wal, R. S. W., Wang, Y., Zhao, C., and Zwinger, T.: Evolution of the Antarctic Ice Sheet Over the Next Three Centuries From an ISMIP6 Model Ensemble, Earth's Future, 12, e2024EF004 561, https://doi.org/https://doi.org/10.1029/2024EF004561, 2024.

Shepherd, A., Ivins, E., Rignot, E., Smith, B., van den Broeke, M., Velicogna, I., Whitehouse, P., Briggs, K., Joughin, I., Krinner, G., Nowicki, S., Payne, T., Scambos, T., Schlegel, N., A, G., Agosta, C., Ahlstrøm, A., Babonis, G., Barletta, V., Blazquez, A., Bonin, J., Csatho, B., Cullather, R., Felikson, D., Fettweis, X., Forsberg, R., Gallee, H., Gardner, A., Gilbert, L., Groh, A., Gunter, B., Hanna, E., Harig, C., Helm, V., Horvath, A., Horwath, M., Khan, S., Kjeldsen, K. K., Konrad, H., Langen, P., Lecavalier, B., Loomis, B., Luthcke, S., McMillan, M., Melini, D., Mernild, S., Mohajerani, Y., Moore, P., Mouginot, J., Moyano, G., Muir, A., Nagler, T., Nield, G., Nilsson, J., Noel, B., Otosaka, I., Pattle, M. E., Peltier, W. R., Pie, N., Rietbroek, R., Rott, H., Sandberg-Sørensen, L., Sasgen, I., Save, H., Scheuchl, B., Schrama, E., Schröder, L., Seo, K.-W., Simonsen, S., Slater, T., Spada, G., Sutterley, T., Talpe, M., Tarasov, L., van de Berg, W. J., van der Wal, W., van Wessem, M., Vishwakarma, B. D., Wiese, D., Wouters, B., and The IMBIE team: Mass balance of the Antarctic Ice Sheet from 1992 to 2017, Nature, 558, 219–222, https://doi.org/10.1038/s41586-018-0179-y, 2018.

Stevens, C., Robinson, N., O'Connor, G., and Grant, B.: Dynamics of Large Pelagic Ice Crystals in an Antarctic Ice Shelf Water Plume Flowing Beneath Land-Fast Sea Ice, The Cryosphere Discussions, pp. 1–30, https://doi.org/10.5194/tc-2020-249, 2020.

Stokes, C. R., Abram, N. J., Bentley, M. J., Edwards, T. L., England, M. H., Foppert, A., Jamieson, S. S. R., Jones, R. S., King, M. A., Lenaerts, J. T. M., Medley, B., Miles, B. W. J., Paxman, G. J. G., Ritz, C., Van De Flierdt, T., and Whitehouse, P. L.: Response of the East Antarctic Ice Sheet to past and future climate change, Nature, 608, 275–286, https://doi.org/10.1038/s41586-022-04946-0, 2022.

Thomas, R. H.: The Dynamics of Marine Ice Sheets, Journal of Glaciology, 24, 167–177, https://doi.org/10.3189/S0022143000014726, 1979.

Trusel, L. D., Frey, K. E., Das, S. B., Karnauskas, K. B., Kuipers Munneke, P., van Meijgaard, E., and van den Broeke, M. R.: Divergent trajectories of Antarctic surface melt under two twenty-first-century climate scenarios, Nature Geoscience, 8, 927–932, https://doi.org/10.1038/ngeo2563, 2015.

Tsai, V. C., Stewart, A. L., and Thompson, A. F.: Marine ice-sheet profiles and stability under Coulomb basal conditions, Journal of Glaciology, 61, 205–215, https://doi.org/10.3189/2015JoG14J221, 2015.

Weertman, J.: Stability of the Junction of an Ice Sheet and an Ice Shelf, Journal of Glaciology, 13, 3–11, https://doi.org/10.3189/S0022143000023327, 1974.

Wright, A. P., Le Brocq, A. M., Cornford, S. L., Bingham, R. G., Corr, H. F. J., Ferraccioli, F., Jordan, T. A., Payne, A. J., Rippin, D. M., Ross, N., and Siegert, M. J.: Sensitivity of the Weddell Sea sector ice streams to sub-shelf melting and surface accumulation, The Cryosphere, 8, 2119–2134, https://doi.org/10.5194/tc-8-2119-2014, 2014.

Yousefi, M., Wan, J., Pan, L., Gomez, N., Latychev, K., Mitrovica, J. X., Pollard, D., and DeConto, R. M.: The Influence of the Solid Earth on the Contribution of Marine Sections of the Antarctic Ice Sheet to Future Sea-Level Change, Geophysical Research Letters, 49, e2021GL097 525, https://doi.org/10.1029/2021GL097525, 2022.